

Recursive anisotropy: A spatial taphonomic study of the Early Pleistocene vertebrate assemblage of Tsiotra Vryssi, Mygdonia Basin, Greece

Abstract

Spatial taphonomy complements the traditional taphonomic approach. By applying advanced spatial statistical methods, it aims to investigate the multiscale and multi-level spatial properties of biostratinomic and diagenetic processes. In this study, we elaborate on a specific aspect - spatial anisotropy - of taphonomic processes. Circular statistics are used for the fabric analysis of elongated elements; geostatistics (directional variograms), wavelet and point pattern analyses are applied for detecting anisotropy at the assemblage level. The anisotropy of magnetic susceptibility of sedimentary magnetic minerals is as well investigated. This study aims to unravel the taphonomic history of the Early Pleistocene vertebrate assemblage of Tsiotra Vryssi (Mygdonia Basin, Macedonia, Greece), with respect to the specific depositional environment, the number of depositional events (single or multiple) and the degree of transportation of the fossil record (autochthonous vs. allochthonous assemblage). The results of our multiscale and multilevel analysis of anisotropy, integrated with preliminary remarks about the differential preservation of skeletal elements, sedimentological and micromorphological observations, suggest multiple dispersion events and recurrent spatial re-arrangement of a lag, (peri)autochthonous assemblage, consistent with the cyclical lateral switching of a braided fluvial system. Spatial taphonomy enhances our understanding of taphonomic modification processes, in turn with consequences for palaeoecological reconstructions and biochronological estimates. Furthermore, this study offers an important contribution to the building of a spatial taphonomic referential framework for the interpretation of other fossil vertebrate assemblages, including archaeo-palaeontological ones.

Keywords: Anisotropy, Spatial taphonomy, Taphonomy, Site formation processes, Early Pleistocene, Greece

1. Introduction

2 Since the first definition of taphonomy as “the study of the transition (in all its de-
3 tails) of animal remains from the biosphere into the lithosphere” ([Efremov, 1940](#)), the
4 spatial properties of taphonomic processes received special attention. Concerned about
5 thanatocoenosis, [Efremov \(1940\)](#) indicated as chief part of a taphonomic study, among
6 others, the analysis of “the spatial distribution of animal remains and their distribution
7 relatively to the planes of stratification”. More recent research on early hominid evo-
8 lution ([Behrensmeyer, 1975a](#); [Boaz and Behrensmeyer, 1976](#); [Hill, 1976](#)) extended the
9 original definition of taphonomy beyond its role as a “new branch of paleontology”
10 ([Efremov, 1940](#)) to include also formation and modification processes of the archae-
11 ological record. Despite some misrepresentations in the archaeological adaptation of
12 the original concept (e.g., the ontological difference between natural and cultural for-
13 mation processes; [Domínguez-Rodrigo et al., 2011](#); [Lyman, 2010](#)), in the last decades
14 taphonomy has widened its theoretical and methodological framework towards an inte-
15 grative and multidisciplinary investigation that aims to reconstruct the past in all its de-
16 tails, incorporating any signal of the processes, both natural and cultural, that modified
17 the original properties of the organic and inorganic components ([Domínguez-Rodrigo
et al., 2011](#)).

19 If taphonomy evolved towards an evolutionary and systemic approach that em-
20 braces multiple taphonomic levels of organisation (i.e., basic taphonomic elements,
21 taphonomic groups [taphons], taphonomic populations and taphoclades; [Fernández-
22 López, 2006](#)), likewise, the study of the spatial properties of taphonomic processes
23 extended from the analysis of the spatial distribution of animal remains in relation to
24 the stratigraphic setting, towards a multilevel quantitative investigation of the spatial
25 behaviour of different taphonomic entities (*sensu* [Fernández-López, 2006](#)). Therefore,
26 spatial taphonomy ([Domínguez-Rodrigo et al., 2017](#); [Giusti and Arzarello, 2016](#)), en-
27 compasses the spatial properties of basic entities (i.e., taphonomic elements, constitut-

ing the fossil record), as well as higher level entities (e.g., taphonomic groups or populations). Indeed, at multiple scales and levels of organisation, the spatial patterns observed in any palaeontological or archaeological assemblage retain valuable information about taphonomic accumulation and re-elaboration processes (*sensu Fernández-López et al., 2002*). Spatial taphonomic data, appropriately recorded, can be quantitatively analysed within a statistical framework in order to reliably draw inferences about taphonomic processes, in turn with consequences for palaeoecological reconstructions (Fernández-Jalvo et al., 2011), biochronological estimates and the interpretation of past human behaviours.

In this study, we elaborate on a specific aspect - anisotropy - of the spatial properties of taphonomic entities, with implications for the interpretation of taphonomic processes. Anisotropy, as opposed to isotropy, is generally defined as the property of a process of being directionally dependent. Spatial anisotropic patterns can be seen as products of physical anisotropic processes, such as fluvial or eolian processes, which modified at multiple scales and levels of organisation the original spatial properties of taphonomic entities.

At the level of basic taphonomic elements, anisotropy, expressed as preferential orientation of fossils or artefacts, is among the key variables used for interpreting site formation and modification processes. Especially in terrestrial alluvial environments, anisotropy is one of the proxies traditionally used to discriminate autochthonous vs. allochthonous assemblages (Petraglia and Nash, 1987; Petraglia and Potts, 1994; Schick, 1987; Toots, 1965; Voorhies, 1969, among others). The orientation of elongated elements, prone to preferentially align along the flow direction, would eventually indicate the action of water-flows and suggest substantial transport prior to burial. Nevertheless, anisotropy has been equally documented in authochthonous assemblages subjected to low-energy water-flows (Cobo-Sánchez et al., 2014; Domínguez-Rodrigo et al., 2012, 2014d); hence, it can be a necessary but not sufficient condition to differentiate allochthony from autochthony (Lenoble and Bertran, 2004). Moreover, besides water-flow processes, anisotropy has been as well observed in association with a wide range of other biostratinomic processes, such as slope processes (Bertran and Texier, 1995) and trampling (Benito-Calvo et al., 2011).

59 Although the anisotropy of basic taphonomic elements have been long studied,
60 the anisotropy of higher level taphonomic entities received by far less attention (see
61 [Markofsky and Bevan, 2012](#) for a directional analysis of archaeological surface distri-
62 butions). Here we address this research gap and conduct a spatial taphonomic study
63 of anisotropy both at the level of fossil specimens and at the assemblage level. The
64 present study uses a comprehensive set of spatial statistics (fabric analysis, geostatis-
65 tics, wavelet analysis, point pattern analysis) in order to identify directional trends that
66 may not be readily apparent. Indeed, beyond the traditional approach of eye-spotting
67 spatial patterns, spatial statistics allow one to adopt a more formal, quantitative ap-
68 proach.

69 Furthermore, at the scale of sedimentary particles, anisotropy is investigated by
70 means of anisotropy of magnetic susceptibility (AMS). AMS refers to the property of
71 elongated magnetic crystals to orient parallel to the flow direction when transported
72 as sedimentary clasts. In sedimentology, AMS analysis is widely applied in order
73 to determine paleoflows in a range of depositional environments, including turbidite
74 systems, contouritic drifts, beaches, deltas and tidal flats ([Felletti et al., 2016](#); [Liu et al.,](#)
75 [2001](#); [Lowrie and Hirt, 1987](#); [Novak et al., 2014](#); [Parés et al., 2007](#), among others).

76 Therefore, integrating the results of our multiscale and multilevel analysis of anisotropy
77 with preliminary remarks about differential taphonomic preservation, sedimentologi-
78 cal and micromorphological observations, we aim to disentangle the taphonomic his-
79 tory of the fossiliferous locality Tsiotra Vryssi (Mygdonia Basin, Macedonia, Greece;
80 [Konidaris et al., 2015](#)).

81 Finally, this study offers an important contribution to the building of a spatial tapho-
82 nomic referential framework for the interpretation of other fossil vertebrate assem-
83 blages, including archaeo-palaeontological ones ([Domínguez-Rodrigo et al., 2017](#)).

84 **2. The palaeontological site of Tsiotra Vryssi (TSR)**

85 The locality Tsiotra Vryssi (TSR) is located in the Mygdonia Basin (Macedonia,
86 Greece), about 45 km Southeast of Thessaloniki (Fig. 1). TSR was discovered in 2014
87 by a joint research team from the Aristotle University of Thessaloniki and the Eberhard

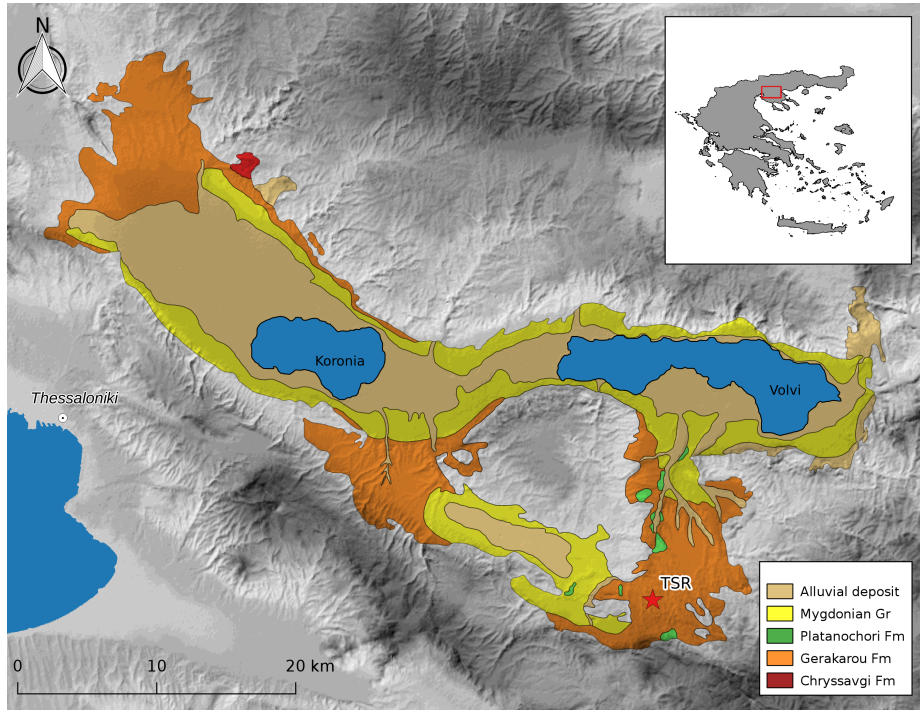


Figure 1: Geological setting of the Mygdonia Basin (Macedonia, Greece) showing the Quaternary and Neogene lithostratigraphic units and the location of Tsiotra Vryssi (TSR), modified after [Koufos et al. \(1995\)](#)

88 Karls University of Tübingen during systematic field surveys in the basin. After the first
 89 collection of fossils from the exposed natural section and the test excavation carried
 90 out in 2014, systematic excavation of the site took place in 2015 and is still ongoing
 91 (Fig. 2a).

92 To date, the excavation covers an about 10 m-thick stratigraphic interval from the
 93 upper Gerakarou Formation (Fig. 1), a suite of continental clastic deposits of mainly
 94 fluvial origin and inter-layered paleosols ([Konidaris et al., 2015; Koufos et al., 1995](#)).
 95 The TSR fauna occurs mainly within a c. 1 m-thick interval of silts (uppermost part
 96 of unit Geo2, see Fig 3) and comprises several mammalian taxa, as well as some birds
 97 and reptiles, whose preliminary biochronological correlation is consistent with a late
 98 Villafranchian (Early Pleistocene) age ([Konidaris et al., 2016, 2015](#)).

99 The sedimentary character of the excavated deposits allows identifying two main

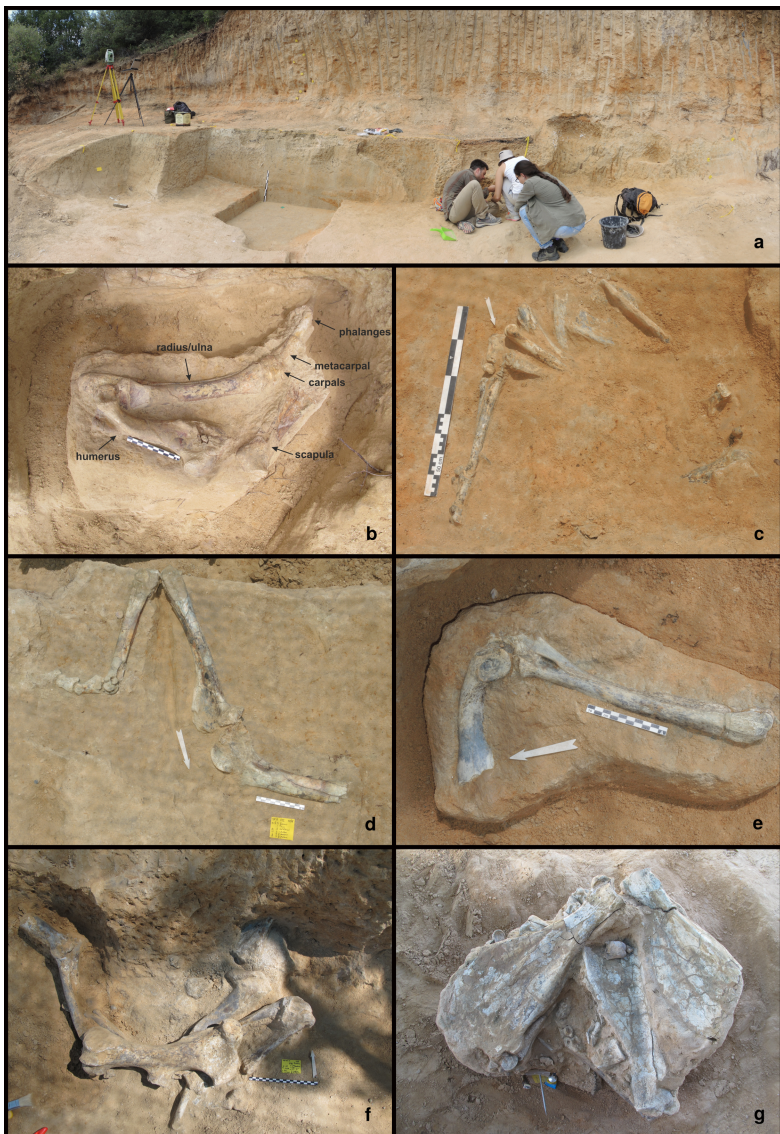


Figure 2: Panoramic view (2017) of the excavation area of Tsiotra Vryssi. Pictures of articulated specimens (a, b, c, d) and clusters of bones (e, f).

100 depositional units (Geo 1 and Geo 2, from younger to older; Fig. 3). The fossiliferous
101 unit Geo 2 begins with about 1.5 m (Geo 2b in Fig. 3) of cross-stratified gravelly
102 sands organised into dm-thick beds with a range of planar to trough-cross laminations.
103 Noteworthy, Geo 2b can be followed laterally for at least 150m in the E-W direction,
104 suggesting an extensive setting of deposition. Above a sharp contact, a few tens of
105 cm of well-sorted, structure-less fine sands follow, which rapidly grade upward into
106 the deposit forming the matrix of the main TSR fossil assemblage (Geo 2a in Fig. 3).
107 This is represented by about 1 m of poorly sorted silts (moderately rich in mica grains),
108 locally intercalated by cm-thick lenses of medium-coarse sands and relatively more
109 clayey in their topmost 30 cm. Apart for alignment of isolated sand to granule grade
110 clasts and some crude parallel lamination in coarse lenses, the deposits appear overall
111 structure-less. Most of Geo 2a is typified by a very pale brown color with a few (less
112 than 10%) pink to reddish yellow mottles, whereas the topmost part of Geo 2a has a
113 strong brown to dark yellowish brown matrix with about the 15-20% of reddish yellow
114 mottles. This change in color is associated with the occurrence of very small calcareous
115 nodules and common to abundant Mn-Fe-bearing nodules with diameter less than 1 cm
116 (see micromorphological analysis in Section 4.5).

117 Geo 1b is represented by an up to 2 m-thick bed set of cross-stratified gravelly
118 sands and gravels, similar to those observed in Geo 2b (Fig. 3). It sits on top of a basal
119 erosion, down-cutting deeply into older sediments (Geo 2a) and shallowing toward the
120 West. In the same direction, the Geo 1b beds tend to be thinner, finer grained and
121 less extensive laterally, suggesting less energetic hydrodynamic conditions. Though
122 poorly exposed, the younger Geo 1a is represented by a monotonous 3 m-thick section
123 of poorly silty sands devoid of coarse intercalations, which rapidly grades into clayey
124 silts of a distinctive pale brown colour.

125 Overall, the stratigraphic position of TSR in the fluviotrestrial Gerakarou Forma-
126 tion ([Koufos et al., 1995](#)) and the specific sedimentary sequence of the site indicate
127 that the TSR assemblage formed in a relatively low energy fluvial environment. A pre-
128 liminary visual inspection of the vertical and horizontal distribution of the fossil finds
129 (Fig. 4) suggests a densely preserved association of fossils (about 24 elements/m²), ho-
130 mogeneously distributed within the study area. Apparent anisotropy is also suggested

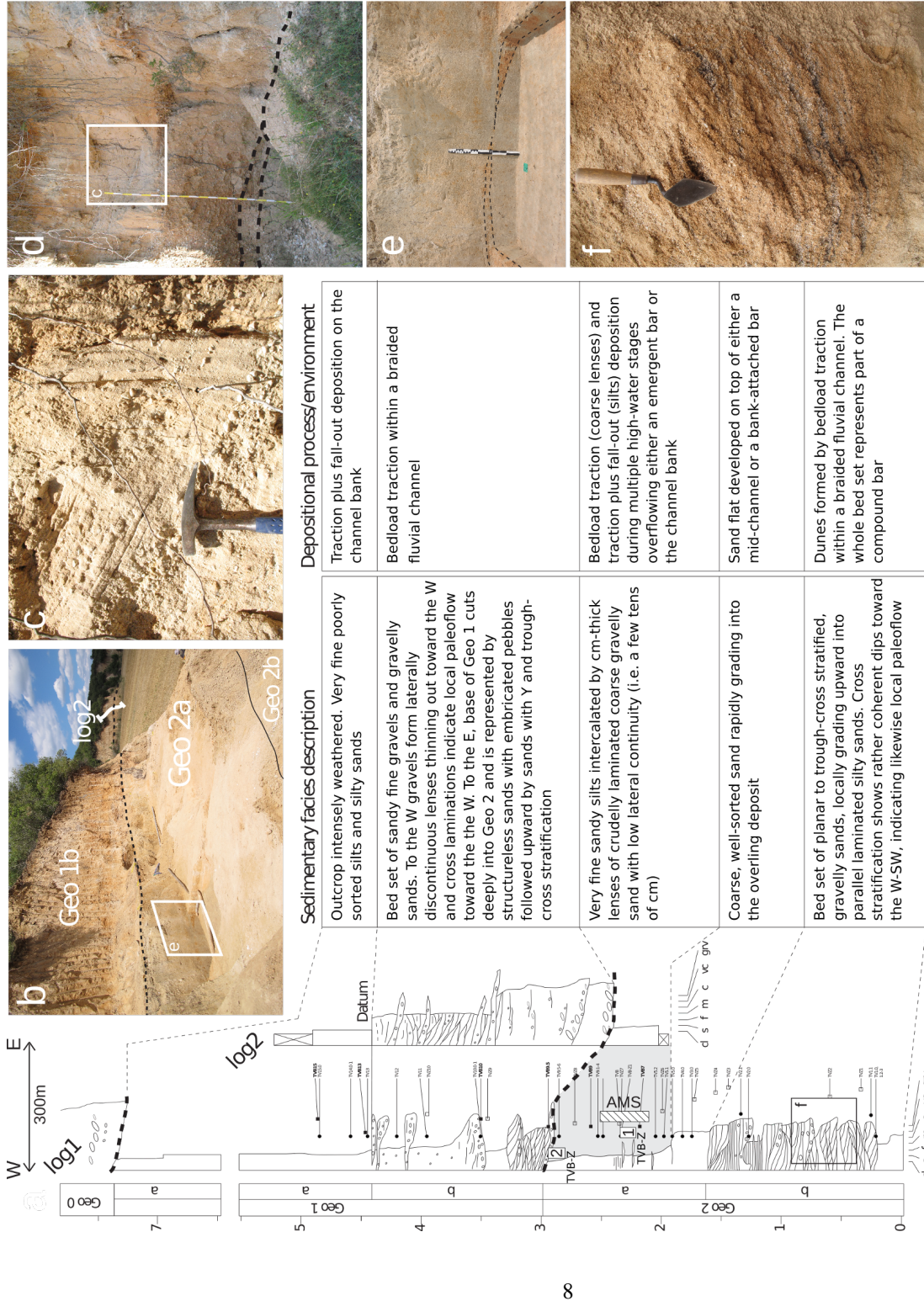


Figure 3: Stratigraphic sedimentary logs (log1 and log 2) with location of main erosional surfaces bounding depositional units Geo 1 and Geo 2, block samples TVB-Z 1 and 2 collected for micromorphology analysis and interval sampled for anisotropy of magnetic susceptibility analysis (AMS); b) WNW-ESE oriented panoramic view of the excavation site and location of the stratigraphic log2 in the background; c) and d) are details of the lower half of log2 showing the basal erosion of Geo 1b followed upward by inclined laminations; e) the middle part of Geo 2a (i.e., the fossiliferous unit) sampled for AMS analysis. Note the presence of cm-thick sand lenses with Fe-hydroxide stains; f) detail of cross stratifications from the top of Geo 2b.

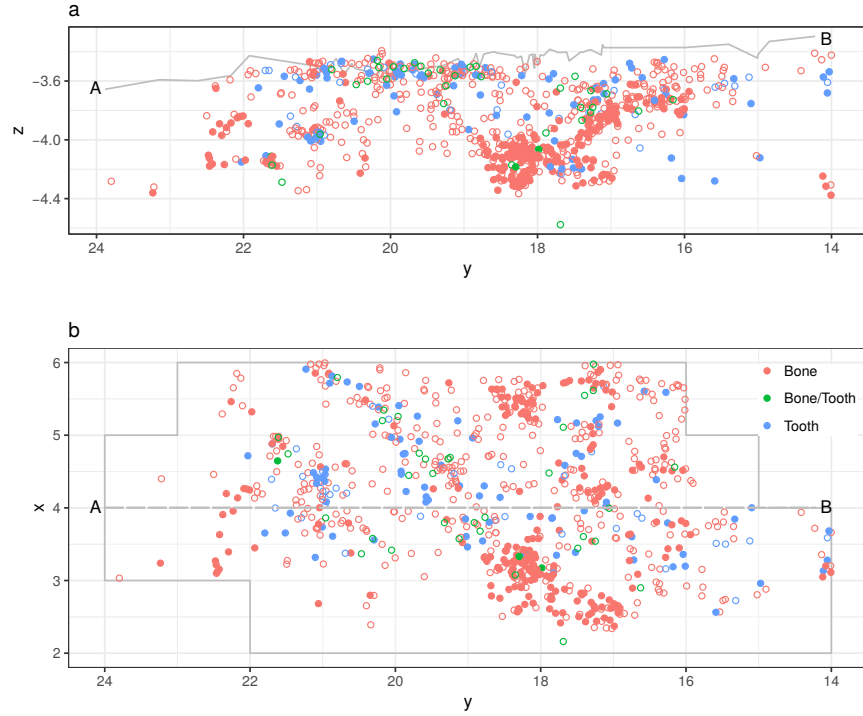


Figure 4: Vertical (a) and horizontal (b) distribution of the sampled fossil specimens from Tsiotra Vryssi (excavations 2015-2017). Filled circles mark complete specimens, hollow circles mark fragmented ones. Grey continuous line in a) marks the Geo 1/2 erosional contact, as recorded at the AB transect marked in b).

131 at assemblage level.

132 In such a fluvial depositional context, questions arise with respect to the specific
 133 character of the TSR fossil assemblage, the number of depositional events (single or
 134 multiple) and the degree of transportation of the fossil record (autochthonous vs. al-
 135 lochthonous assemblage).

136 **3. Material and methods**

137 *3.1. Data collection and subsetting*

138 Since 2015 a grid of 1 m² units was set up and a total station was used in or-
 139 der to record the spatial provenience of collected (i.e., diagnostic bones and teeth,

and carnivore modified bones) and not collected remains (i.e., not diagnostic bone fragments with length \geq 50 mm; Fig. 2a). Not diagnostic, or not carnivore modified bone fragments with length $<$ 50 mm were not recorded. This dimensional threshold was chosen because small bone fragments show more random orientations than longer specimens (Domínguez-Rodrigo et al., 2014d). Orientation (plunge and bearing) of clearly elongated specimens (i.e., specimens with length at least twice the width) was measured with a 1 degree accuracy, using a compass and inclinometer (Eberth et al., 2007; Fiorillo, 1991; Voorhies, 1969, among others). Strike and dip measurements were taken along the symmetrical longitudinal a-axis (SLA) of the specimens (Domínguez-Rodrigo and García-Pérez, 2013), using the lowest endpoint of the a-axis as an indicator of the vector direction. The dimensions (length and maximum width) of the recorded finds were measured on-site with a millimetric measuring tape.

The present spatial taphonomic study analysed a sample of stratified specimens ($n = 797$) from the fossiliferous unit Geo 2a, whose spatial coordinates were recorded with the total station. The area of analysis concerns the 34 m² excavated from 2015 until 2017. The sample included mostly macromammal remains ($n = 707$, 89%), undetermined isolated bone fragments ($n = 70$), birds ($n = 12$) and turtle ($n = 8$) remains. A sub-sample ($n = 249$) was further subset for the fabric analysis described below. Stratified specimens from Geo 2a collected during the test excavation of 2014, or subsequently found in plaster-jackets with concentration of bones during the lab preparation were excluded due to the lack of precise spatial coordinates. The very small sample ($n = 4$) of micromammal remains was also not included in the spatial and faunal analyses. Faunal analysis was conducted on a sub-sample of complete or fragmented, isolated or articulated macromammal remains ($n = 707$). Further subsetting strategies are described below.

As for the AMS analysis, we collected 18 cylindrical oriented samples ($\varnothing = 2.5$ cm) from the middle part of the fossiliferous unit Geo 2a (Fig. 3). AMS analysis was performed at the Alpine Laboratory of Paleomagnetism in Peveragno (Italy) using a AGICO KLY-3 Kappabridge susceptibility meter (15-positions, manual oriented).

In order to investigate the micromorphological properties of the Geo 2a unit (i.e., sedimentary structures and pedogenetic features), two blocks of undisturbed sediment

¹⁷¹ were collected from the excavation area; one (TVB-Z 1) from the middle part and
¹⁷² the other (TVB-Z 2) from the topmost 30 cm of the unit (Fig. 3). The blocks were
¹⁷³ later consolidated for preparation of thin sections following the methods described in
¹⁷⁴ Murphy (1986).

¹⁷⁵ *3.2. Spatial anisotropy*

¹⁷⁶ Different methods have been developed in neighbouring disciplines to detect spa-
¹⁷⁷ tial anisotropy. Here we use circular statistics for the fabric analysis of taphonomic el-
¹⁷⁸ ements; geostatistics (directional variograms), wavelet analysis and point pattern anal-
¹⁷⁹ ysis for detecting anisotropy at the assemblage level.

¹⁸⁰ *3.2.1. Fabric analysis*

¹⁸¹ The first controlled experiments and analyses of the orientation and dispersal of
¹⁸² disarticulated mammal bones as indicators of the depositional context, carried out by
¹⁸³ Toots (1965) and Voorhies (1969), led to an increasing number of studies of the effects
¹⁸⁴ of water flows on natural and anthropogenic faunal assemblages (Aramendi et al., 2017;
¹⁸⁵ Benito-Calvo and de la Torre, 2011; Cobo-Sánchez et al., 2014; de la Torre and Benito-
¹⁸⁶ Calvo, 2013; Domínguez-Rodrigo et al., 2014a, 2012, 2014d; Fiorillo, 1991; Nash and
¹⁸⁷ Petraglia, 1987; Organista et al., 2017; Petraglia and Nash, 1987; Petraglia and Potts,
¹⁸⁸ 1994; Schick, 1987, among others).

¹⁸⁹ Whereas most of these studies have been conducted on disarticulated long bones
¹⁹⁰ or elongated bone fragments - which were observed to preferentially align their a-
¹⁹¹ axes along the direction of the flow - relatively few have investigated the hydraulic
¹⁹² behaviour of articulated skeletal elements. Flume experiments conducted by Coard
¹⁹³ and Dennell (1995) and Coard (1999) demonstrated that articulated bones display a
¹⁹⁴ greater transport potential than disarticulated ones when the articulated elements align
¹⁹⁵ themselves. However, they also noted that skeletal parts with a higher number of artic-
¹⁹⁶ ulated elements, such as complete limbs, may show weak preferential orientation when
¹⁹⁷ assuming disorganised spatial configuration, i.e., when not aligned. Therefore, articu-
¹⁹⁸ lated bones, although relatively common in TSR (Fig. 2a,b,c,d), were not included in
¹⁹⁹ the fabric analysis.

200 In this study we applied circular statistics to a subset of 249 non-articulated, elongated bone specimens, having length $\geq 20\text{mm}$ ([Domínguez-Rodrigo et al., 2014d](#)).
201 No distinction of skeletal elements was made, due to the high percentage (91%, $n = 227$) of fragmented remains in the analysed sample - mostly appendicular ($n = 122$),
202 undetermined ($n = 93$), axial and cranial ($n = 12$) fragments - and due to the low per-
203 centage (9%, $n = 22$) of complete bones - 17 limb bones, 4 scapulae and a rib.
204

205
206 We applied Rayleigh and omnibus tests of uniformity, such as Kuiper, Watson and
207 Rao ([Jammalamadaka et al., 2001](#)), to test the isotropic orientation of the fossil speci-
208 mens. Whereas the Rayleigh test assumes a unimodal distribution and assess the sig-
209 nificance of the sample mean resultant length (\bar{R}), the omnibus tests detect multimodal
210 departures from the null hypothesis of circular isotropy.

211
212 Rose and equal area Schmidt diagrams were used as exploratory data analysis tools
213 to visualise the sample distribution. Compared to the widely used rose diagrams, which
214 plot the circular distribution of the bearing values, the Schmidt equal area diagram
215 informs about the distribution of the three-dimensional orientation (plunge and bearing)
216 of the elements ([Fiorillo, 1988](#)). Points plotting at the margin of the globe indicate
217 planar fabric, whereas points towards the centre have higher dip angles.

218
219 The Woodcock diagram ([Woodcock and Naylor, 1983](#)), based on three ordered
220 normalised eigenvalues (S_1, S_2, S_3), was used to discriminate between linear (cluster),
221 planar (girdle) and isotropic distributions. In the Woodcock diagram, the C parameter
222 ($C = \ln(S_1/S_3)$) expresses the strength of the preferential orientation, and its signifi-
223 cance is evaluated against critical values from simulated random samples of different
224 sizes. A perfect isotropic distribution would plot at the origin, with equal eigenvalues
225 ($S_1 = S_2 = S_3 = 1/3$). On the other hand, the K parameter ($K = \frac{\ln(S_1/S_2)}{\ln(S_2/S_3)}$) expresses
226 the shape of the distribution, and it ranges from zero (uni-axial girdles) to infinite (uni-
227 axial clusters).

228
229 In a fluvio-lacustrine environment a cluster distribution would suggest a strong
230 preferential orientation of the sample, such as in the case of channelised water flows
231 ([Petricchia and Potts, 1994](#)), whereas a girdle distribution a weaker preferential orienta-
232 tion, spread over a wider range of directions. Overland flows have been interpreted to
233 produce such a pattern ([Organista et al., 2017](#)). On the other hand, a isotropic distribu-

tion would suggest that post-depositional disturbance by water flows was not strong enough to preferentially orient the assemblage (Domínguez-Rodrigo et al., 2014a). However, a variety of taphonomic processes can produce similar patterns. Fabric analysis, although very informative, has low power by itself. In order to overcome the intrinsic limitations of the fabric analysis, a multivariate approach to site formation and modification processes should be employed (Lenoble and Bertran, 2004).

3.2.2. Geostatistics

Geostatistics refer to a body of concepts and methods typically applied to a limited sample of observations of a continuous variable, such as environmental variables. Geostatistics thus aim to estimate the variance and spatial correlation of known observations and predict, using interpolation methods such as Kriging, unknown values of the variable at non-observed locations. Moreover, by using directional variograms, geostatistics enable the identification of spatial anisotropy (i.e., directional patterns). Since the vast majority of spatial statistics assume stationarity and isotropy, it is well understood that a misinterpretation of spatial anisotropy may result in inaccurate spatial modelling and prediction.

Although well known in ecological studies, only a relatively small number of studies have explicitly applied geostatistics to the study of site formation and modification processes, using directional variograms to investigate the specimens size spatial distributions (Domínguez-Rodrigo et al., 2014a,c), or to specifically detect spatial anisotropy of archaeological assemblages (Bevan and Conolly, 2009; Markovsky and Bevan, 2012).

In order to investigate spatial anisotropy in the distribution of the TSR fossil assemblage and identify spatial continuity in some directions more than others, we used directional variograms and variogram maps. The studied sample includes 797 recorded specimens (isolated or articulated, complete or fragmented bones and teeth) unearthed from Geo 2a and included in the 34 m² window of analysis (Fig. 4). The same sample was used for the wavelet and point pattern analyses.

Specifically, plotting the semi-variance between the variable values of sampled point pairs as a function of distance (spatial lag) between these pairs, directional var-

iograms are used to model the spatial variation at multiple scales and different directions. Three parameters (*nugget*, *range* and *sill*) are estimated from an experimental variogram to fit a theoretical omnidirectional variogram. The *nugget* is used to account for spatial variability at very short distances. The *range* indicates the maximal distance up to which there is spatial correlation. At longer distances the semi-variance levels off forming the *sill*, indicating independence between pairs of sample separated by that minimum distance (Dale and Fortin, 2014; Lloyd and Atkinson, 2004). Thus, we plotted the experimental directional variogram against the theoretical omnidirectional variogram. A directional semi-variance lower than the fitted omnidirectional variogram indicates continuity in the analysed direction. We selected for our analysis the N-S (0°), E-W (90°), NE-SW (45°) and NW-SE (135°) geographical directions. In addition to the directional variograms, variogram maps are visual representations of the semi-variance: the anisotropy is represented by an ellipse, its axes being proportional to the variation expected in each direction. Thus, the direction of maximum anisotropy corresponds with the major axis of the ellipse (Legendre and Legendre, 2012).

3.2.3. Wavelet analysis

As a second method for the detection of spatial anisotropy at the assemblage level we used the wavelet analysis. Wavelet analysis, commonly applied in mathematics for signal processing, has relatively wide application in palaeoclimatology and palaeoecology, but is seldom used in site formation processes studies (Markovsky and Bevan, 2012).

Differently from the geostatistics approach to the analysis of spatial anisotropy, which is based on a transformation of point values into a continuous surface, the wavelet approach does not apply any transformation, but identifies the elements (points) of a pattern merely by their location. In this regard, the wavelet analysis does not suffer from the arbitrary choice of a surface smooth parameter, as in the case of geostatistics.

For each specific point of the pattern, a wheel of 360 sectors of 1° is used to measure the average variance in the angles between point pairs (Rosenberg, 2004). The significance of the wavelet analysis is evaluated against 199 Monte Carlo simulations of the observed pattern under the null hypothesis of randomness. The variance is plotted as a

function of angle measurements. Direction is measured anti-clockwise from East (i.e., 0° is East, 90° is North). When the distribution of the observed values (dashed line) wanders above the simulated values (continuous line), the pattern shows significant anisotropy in that direction.

3.2.4. Point pattern analysis

A spatial point pattern is the outcome of a random spatial point process. Any natural phenomenon which results in a spatial point pattern, such as a distribution pattern of fossils, can be viewed as a point process (Baddeley et al., 2015). Therefore, the analysis of a spatial point pattern ultimately addresses the nature of the point process that generated the pattern. Point pattern analysis has been specifically applied to the study of site formation and modification processes by a relatively small number of studies (Domínguez-Rodrigo et al., 2014a, 2017, 2014c; Giusti and Arzarello, 2016; Giusti et al., in press; Lenoble et al., 2008; Organista et al., 2017). However, this analytical method has never been used to detect anisotropy in the distribution patterns of archaeological or palaeontological assemblages. Nevertheless, detecting anisotropy is an essential part of any spatial analysis. Standard statistical tools in spatial point pattern analysis rely on crucial assumptions about the point process itself: a point process is assumed to be stationary and/or isotropic if its statistical properties are not affected by shifting and/or rotating the point process.

In order to further assess the presence of anisotropy in the distribution pattern of the TSR assemblage, we specifically applied the point pair distribution function ($O_{r1,r2}(\Phi)$; Baddeley et al., 2015). The function estimates the probability distribution of the directions of vectors joining pairs of points that lie more than $r1$ and less than $r2$ units apart. With selected different distances $r1$ and $r2$, the function estimates the multiscale variation of anisotropy. Results are visualised in rose diagrams, where the direction is measured counter-clockwise from East (0°).

At the supra-element assemblage level, spatial anisotropy is expected to be detected in a fluvial depositional environment, and most likely to share the same preferential orientation with taphonomic elements. Characteristic elongated lag deposits are typical patterns observed in association with water-flows dragging materials in one direction,

321 the same as the main orientation of the elements (Domínguez-Rodrigo et al., 2012).

322 *3.3. Anisotropy of magnetic susceptibility (AMS)*

323 The anisotropy of magnetic susceptibility (AMS) is a technique used to identify
324 preferred orientation of magnetic minerals in rocks and unconsolidated sediments (Hrouda,
325 1982; Tarling and Hrouda, 1993). It is based on the principle that, when a magnetic
326 field is applied to a sample, the induced magnetization depends on the bulk orienta-
327 tion of its magnetic constituents. In turn, the AMS magnitude depends on both the
328 anisotropy of individual magnetic particles and the degree of their alignment. Particle
329 anisotropy can be related to either crystalline (anisotropy along a specific crystal plane
330 or axis) or shape (anisotropy along the long axis of the particle) characteristics. Since in
331 most magnetic minerals forming sedimentary particles the long crystallographic axis is
332 the easiest to magnetize (e.g., magnetite), the shape anisotropy is generally dominant,
333 with few exceptions (e.g., hematite).

334 The magnetic susceptibility is represented by three symmetric tensors describing
335 an ellipsoid with three susceptibility axes named K1 to K3 and ordered by decreasing
336 susceptibility. The orientation of the ellipsoid is evaluated projecting the ellipsoid axes
337 on an equal-area projection stereogram. Thus, the shape of the ellipsoid is evaluated
338 using the Flinn or Jelinek scatter plots. In a Flinn (F/L) diagram the foliation along
339 the horizontal axis ($F = K2/K3$; Stacey et al., 1960) is plotted against the lineation
340 along the vertical axis ($L = K1/K2$; Balsey and Buddington, 1960). Values of $F/L < 1$
341 indicate oblate ellipsoids (i.e., disc-shaped), whereas values of $F/L > 1$ indicate prolate
342 ellipsoids (i.e., cigar-shaped) with the axial ratios increasing with increasing distance
343 from the origin. Alternatively, the AMS magnitude and shape can be visualized on the
344 Jelinek shape plot (Jelinek, 1981), by using the corrected anisotropy degree

$$Pj = \exp \sqrt{2[(\ln K1 - k)^2 + (\ln K2 - k)^2 + (\ln K3 - k)^2]}$$

345 where

$$k = \frac{\ln K1 + \ln K2 + \ln K3}{3}$$

346 and the shape parameter

$$T = \frac{\ln L - \ln F}{\ln L + \ln F}$$

347 where samples are prolate for $-1 < T < 0$ or oblate for $0 < T < 1$.

348 In sediments, oblate ellipsoids with imbrication angles less than 20° are considered
349 diagnostic of primary depositional processes (Hamilton and Rees, 1970; Hrouda, 1982;
350 Lanza and Meloni, 2006; Liu et al., 2001; Tarling and Hrouda, 1993). In turn, prolate
351 ellipsoids mostly relate to post-depositional deformation (e.g., rocks recording tectonic
352 or metamorphic strain), especially when the magnetic anisotropy is high (Hrouda and
353 Janák, 1976).

354 *3.4. Differential preservation*

355 Differential preservation, or taphonomic survival, refers to the proportion of tapho-
356 nomic elements being preserved after the action of environmental factors (Fernández-
357 López, 2006). Selective preservation arises from the differential modification of tapho-
358 nomic entities, by interaction of inherent properties of the entities with the external
359 environmental factors. Skeletal part representation is among the key variables poten-
360 tially indicative of the selective action of water-flows (Behrensmeyer, 1975b; Kauf-
361 mann et al., 2011; Voorhies, 1969, among others). Other variables, not considered
362 in this preliminary study, include breakage patterns, disarticulation patterns and bone
363 surface modifications.

364 The pioneering flume experiments by Voorhies (1969) on disarticulated, complete
365 sheep and coyote bones resulted in a three-group classification of fluvial transport sus-
366 ceptibility of skeletal elements, subsequently elaborated by Behrensmeyer (1975b).
367 Since shape and structural density have been found to influence the transportability of
368 skeletal elements (Behrensmeyer, 1975b; Boaz, 1982), assemblages subject to moder-
369 ate to high-energy water-flows typically show an under-represented number of smaller,
370 less dense bones. The Voorhies Groups I (rib, vertebra, sacrum, sternum) is the most
371 easily affected by fluvial transport; thus its presence or absence in the fossil assemblage
372 informs about the degree of disturbance by water-flows. In turn, the proportion between
373 the represented Voorhies Groups provides evidence for the degree of preservation of the

374 assemblage ([Behrensmeyer, 1975b](#)). We included in the Voorhies groups only com-
375 plete, non-articulated macromammal bones (plus rami of mandibles, and maxillae) of
376 adult individuals - the very few specimens of juvenile individuals, having different hy-
377 draulic behaviour, were excluded. Our grouping criteria followed the classification
378 reported in [Lyman \(1994, Tab.6.5\)](#). Carpals, tarsals and sesamoids were included in
379 Voorhies Group I/II, as the phalanges; maxillae in Group II/III, as the mandibular rami.
380 The studied sample included 147 specimens of Perissodactyla (n = 59), Artiodactyla
381 (n = 41), Carnivora (n = 12) and yet indeterminate taxa (n = 35). The distribution of
382 determinate Voorhies Groups was further categorised in 5 size classes, following the
383 body mass (BM) classification of [Palombo \(2010, 2016\)](#), modified for *Ursus etruscus*
384 after [Koufos et al. \(in press\)](#). The first group (BM1), not present so far in our collec-
385 tion, includes mammals whose weight is less than 10 kg; BM2 ranges from 10 to 59
386 kg (*Canis etruscus*); BM3 from 60 to 249 kg (*Ursus etruscus*, medium-sized Cervi-
387 dae); BM4 from 250 to 1000 kg (*Equus*, *Bison*, *Praemegaceros*). We excluded from
388 the Voorhies Groups specimens attributed to BM5, that includes very large mammals
389 over 1000 kg weight (Rhinocerotidae and Elephantidae). Nevertheless, their skeletal
390 element representation was analysed following the Fluvial Transport Index (FTI) clas-
391 sification of [Frison and Todd \(1986\)](#). Undetermined taxa or BM classes - yet in the
392 BM2-BM4 range - (named NA) were also included in the analysis.

393 Closely related to the Voorhies Groups, the ratio of complete isolated teeth/vertebrae
394 (T/V) is another indicator of the depositional environment ([Behrensmeyer, 1975b](#)).
395 High-energy fluvial deposits, such as channel-fills and -lag deposits, tend to have high
396 T/V ratio, whereas a low T/V ratio characterises low-energy fluvial deposits, such as
397 that of floodplain deltaic and lacustrine settings ([Lyman, 1994](#)).

398 Complimentary to the hydraulic behaviour of complete, isolated faunal remains
399 classified in the Voorhies Groups, the skeletal part representation of fragmented bones
400 provides another indication of the degree of preservation of the assemblage ([Domínguez-](#)
401 [Rodrigo et al., 2017, 2014d; Pante and Blumenschine, 2010](#)). Vertebrae and ribs, being
402 mostly cancellous, fragile and comparatively low-dense bones, are more susceptible to
403 fragmentation and transportation, even in low-energy conditions, with respect to cranial
404 and appendicular elements, which are more dense and likely to survive in lag assem-

405 blages (Domínguez-Rodrigo et al., 2017). In order to integrate the Voorhies Groups,
406 we analysed a subsample of 400 isolated macromammal specimens, composed of 315
407 bone and tooth fragments, 78 complete teeth, 1 antler, and 6 appendicular bones of
408 juvenile or BM5 specimens.

409 Finally, the distribution of articulated bones was analysed by anatomical regions. A
410 sub-sample of 50 articulated macromammal units of 154 bone elements were classified
411 as axial (vertebrae, ribs, scapulae and pelvis) or appendicular (humeri, femura, radii,
412 tibiae, metapodials, carpals/tarsals and phalanges) units.

413 *3.5. Reproducible research*

414 The subset of the raw data collected for this study, necessary to reproduce the re-
415 ported results, is licensed, except where otherwise specified, under the CC-BY license
416 and publicly available on an open-access repository at the DOI: [zenodo/osf?](#). The
417 repository includes in addition metadata description and the code used to process and
418 reduce the dataset. The analyses were performed in R: a language and environment
419 for statistical computing ([R Core Team, 2017](#)); except for the wavelet analysis, per-
420 formed using the PASSaGE software, version 2 ([Rosenberg and Anderson, 2011](#)). The
421 commented R code needed to reproduce the reported analyses is released under the
422 MIT license in the same repository. We provide as well a detailed description of the
423 procedure used in PASSaGE.

424 **4. Results**

425 *4.1. Anisotropy of basic taphonomic elements*

426 Circular statistics were applied for the fabric analysis of basic taphonomic ele-
427 ments, i.e., isolated, not articulated elongated complete bone specimens or bone frag-
428 ments. Tab. 1 summarises the results of the circular uniformity tests. The Rayleigh
429 test, which assumes a unimodal distribution, confirmed ($p - value = 0.001$) the sig-
430 nificance of the sample mean resultant length ($\bar{R} = 0.165$). The value of \bar{R} close to 0
431 indicates that the data are evenly spread around the mean direction ($\bar{\theta} = 148$, SE), with
432 relatively high standard deviation ($\hat{\sigma} = 1.89$) and angular variance ($V = 48$). On the

Table 1: Values and p -values of circular uniformity test statistics.

Sample n	mean dir.	Rayleigh		Kuiper		Watson		Rao	
		\bar{R}	p	V_n	p	U^2	p	U	p
249	148°	0.165	0.001	2.3791	<0.01	0.3957	<0.01	186.5181	<0.001

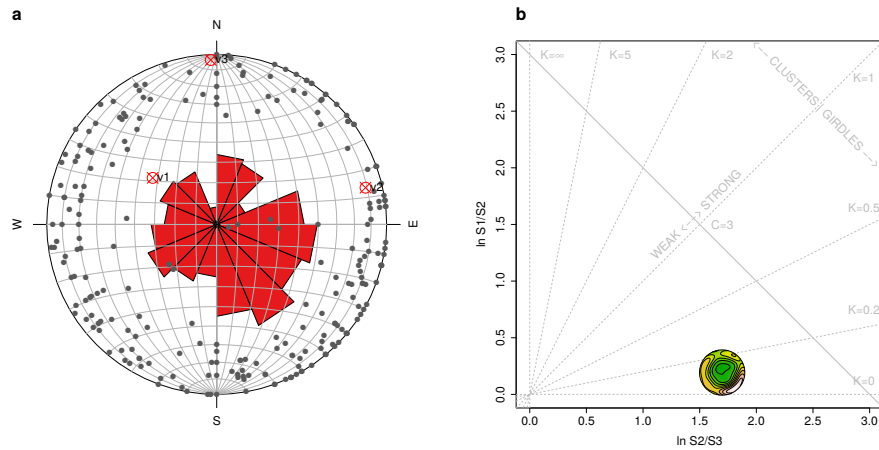


Figure 5: Rose and equal area Schmidt diagrams (a). Woodcock diagram (b).

other hand, the Schmidt and rose diagrams (Fig. 5a) showed a multimodal distribution, mostly concentrated in the SE quadrant and with secondary peaks to the N and SW. Accordingly, the Kuiper, Watson and Rao omnibus tests, all rejected the null hypothesis of uniformity at the 99% confidence level, thus suggesting a significant anisotropic multimodal distribution of the fossil sample. Moreover, the Schmidt diagram (Fig. 5a) showed a planar fabric of the sample distribution, with points plotting predominantly on the edge of the equal area hemisphere, thus indicating 0-to-low degree of dip (mean plunge=12°; variance=1.5°).

In the Woodcock diagram (Fig. 5b), the C value (1.89) is higher than the critical S_1/S_3 test value (1.44) for $N=300$ at 99% confidence level. Thus, the data sample significantly rejects the hypothesis of randomness in favour of a strong organised sample. The K value (0.11) plots the data sample close to $K = 0$, indicating uniaxial girdles (planar fabric).

446 *4.2. Anisotropy of the taphonomic population*

447 Geostatistics (directional variograms and variogram map), wavelet and point pat-
448 tern analyses were used for detecting anisotropy at the assemblage level. Fig. 6a shows
449 the kernel smooth density estimation ($\sigma = 0.17$) of the sample distribution in the study
450 area. A preliminary visual examination suggests a NW-SE oriented clustering of the
451 assemblage, although interfered with secondary NE-SW oriented dispersion. Fig. 6b
452 shows the variograms in the four main geographical directions (N-S, E-W, NE-SW,
453 NW-SE), plotted against the omnidirectional fitted variogram. As a rule of thumb, in
454 order to determine the spatial structure of the sampled data, only the first two-thirds of
455 the variogram are interpreted (Dale and Fortin, 2014). The omnidirectional variogram
456 (red line) indicates that at short distance lags, the semi-variances are close to zero,
457 indicating very strong spatial structure (correlation). With longest distance lags, the
458 semi-variance rise to a plateau (*sill*) of lack of spatial correlation. The semi-variance
459 of the NW-SE (135°) direction is lower than in the omnidirectional variogram, start-
460 ing well before the *sill*, thus indicating continuity (spatial correlation) in that direction.
461 Minor directional trends are also detected in the N-S (0°), and to a lesser extent in the
462 NE-SW (45°) directions. This result is clearly confirmed by the diagonal striping in the
463 variogram map (Fig. 6c). The map shows a major ellipse oriented NW-SE, with minor
464 parallel structures.

465 As for the wavelet analysis, Fig. 7 plots the variance as function of the direction,
466 ranging anti-clockwise from 0° (E) to 180° (W). A major peak is evident at 135° (NW),
467 wandering way above the expected values for a random (isotropic) pattern. A sec-
468 ondary significant peaks, although of much less intensity, is present at 85° (N). In
469 accordance with the directional variograms, the wavelet analysis indicates a signifi-
470 cant anisotropy in the NW-SE direction. Moreover, it suggests minor occurrence of
471 points (specimens) in the N-S direction, as also indicated by the geostatistics analysis.
472 However, in contrast with the directional variograms, the angular wavelet graph does
473 not support significant preferential orientation in the NE range (angles between 0° and
474 90°).

475 Fig. 8 shows the results of our point pattern analysis and specifically the point
476 pair distribution function $O_{r1,r2}(\Phi)$ for a range of distances $r1 = 0.01$ m and $0.25 <$

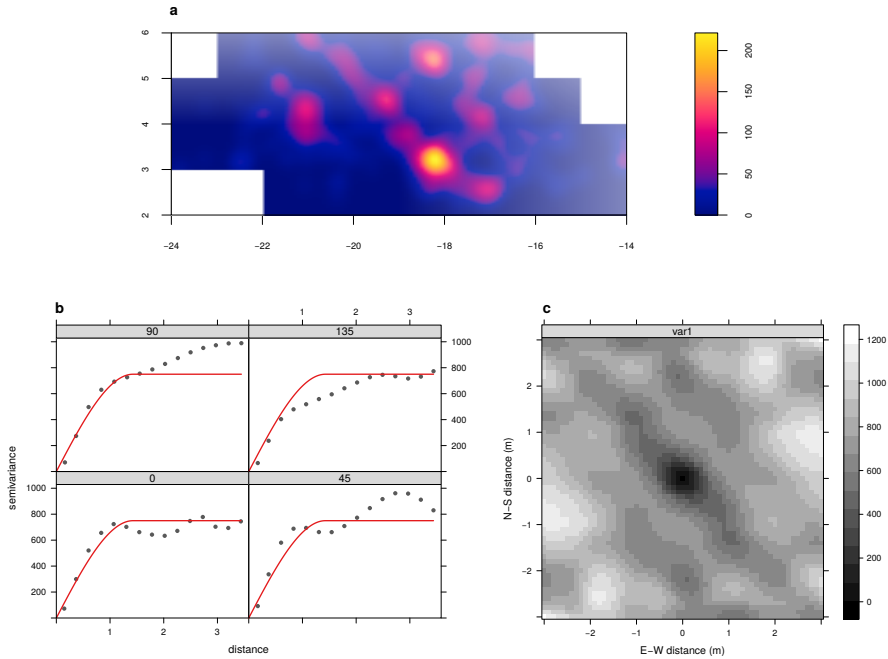


Figure 6: Kernel smoothed intensity function of the fossil assemblage (a). Directional variograms (4 clockwise directions from N-S, 0°) shown as grey points alongside the fitted omnidirectional variogram shown as a continuous red line (b) and variogram map (c).

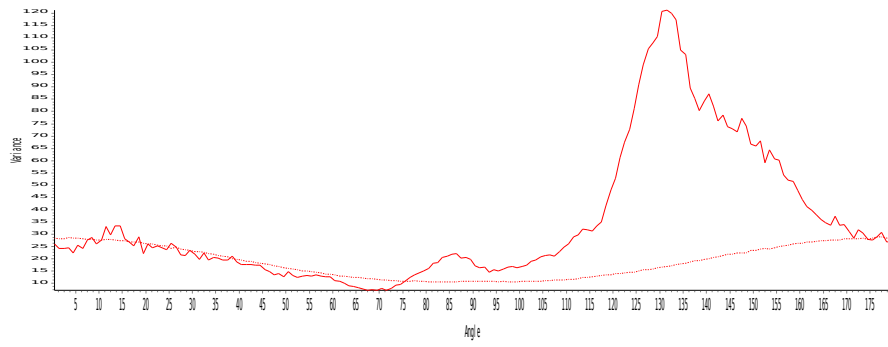


Figure 7: Angular wavelet graph. Angles range from 0° (E) to 180° (W). Peaks of variance (continuous line) indicate the direction of maximum anisotropy. Dashed line marks the Monte Carlo simulated null hypothesis of isotropy.

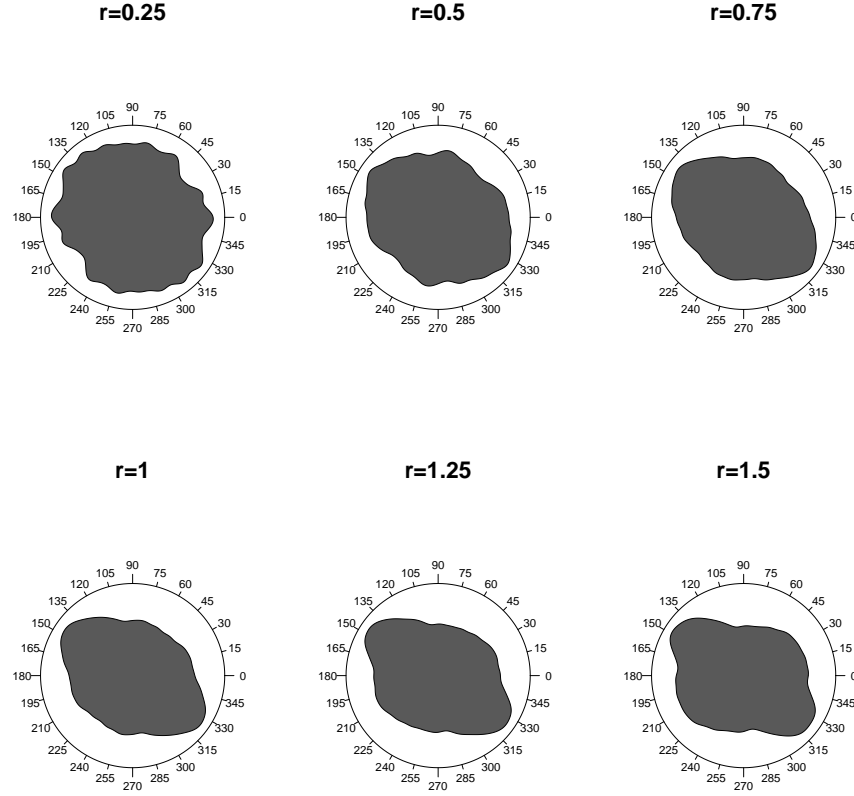


Figure 8: Rose diagrams of the point pair distribution function for a range of distances ($0.25 < r_2 < 1.5\text{m}$). Direction is measured counter-clockwise from East (0°).

477 $r_2 < 1.5\text{ m}$. The plot illustrates the multiscale variation of anisotropy, from a uniform,
 478 isotropic pattern (for $r_2 = 0.25\text{ m}$), to increased anisotropy in the NW-SE direction.
 479 The maximum anisotropy is observed for $r_2 = 1\text{ m}$, as elements at a maximum distance
 480 of 1 m show the strongest directional pattern. With increased distances of $r_2 > 1\text{ m}$, the
 481 rose diagrams suggest the addition of a second orthogonal NE-SW directional trend,
 482 which reflects the parallel alternation of NW-SE bands in the assemblage distribution.

483 4.3. Anisotropy of magnetic susceptibility

484 In Fig. 9a, the AMS of the whole sample set ($n = 18$) is investigated. The equal-
485 area projection of the three susceptibility axes K1-K3 (left-hand side of Fig. 9a) indi-
486 cates high variability of the axes orientation, with confidence angles of the K1 and K2
487 mean directions largely overlapping. This result suggests no preferential orientation
488 of the axes. However, the Flinn and Jelinek plots (right-hand side of Fig. 9a) reveal
489 the presence of 7 samples with prolate ellipsoids, thus suggesting the action of post-
490 depositional deformation processes which could have obliterated the primary deposi-
491 tional pattern. Therefore, in order to overcome possible post-depositional noise, further
492 AMS analysis focused only on a sub-set of samples showing oblate ellipsoids ($n = 11$).
493 In Fig. 9b, the equal-area projection shows a well defined clustering of the axes, with
494 the maximum anisotropy axis K1 aligned along the NW-SE direction and the K3 im-
495 brication angles varying within a wide range of angles (from 4° to 85°). Because high
496 K3 imbrication angles may result from post-depositional rehash of sediments, further
497 analysis were conducted on a selection of 5 samples with K3 imbrication angles less
498 than 20° (Hamilton and Rees, 1970; Hrouda, 1982; Lanza and Meloni, 2006; Liu et al.,
499 2001; Tarling and Hrouda, 1993). In Fig. 9c, the equal-area projection indicates again a
500 NW-SE orientation of the maximum anisotropy axis K1. Despite the small sample size,
501 the AMS analysis suggests a weak anisotropy of magnetic sedimentary grains along a
502 NW-SE direction.

503 4.4. Differential preservation

504 Fig. 10a shows the distribution at the family level of the whole sampled material.
505 Determined taxa included Perissodactyla, Artiodactyla, Carnivora and Proboscidea,
506 together with a number of undetermined bone fragments (44%). The histogram shows
507 the prominent presence of Equidae over other taxa (27%), followed by Bovidae (11%)
508 and Cervidae (5%). However, it is worth noting the presence of very large mammals
509 (body mass class BM5), such as Elephantidae and the rhinocerotid *Stephanorhinus* sp.,
510 and to a less extent, of carnivores, such as *Canis etruscus* and *Ursus etruscus*.

511 The distribution of the Voorhies Groups plotted by body mass classes is shown
512 in Fig. 10b. BM1 is so far not present in the TSR assemblage, while BM2 includes

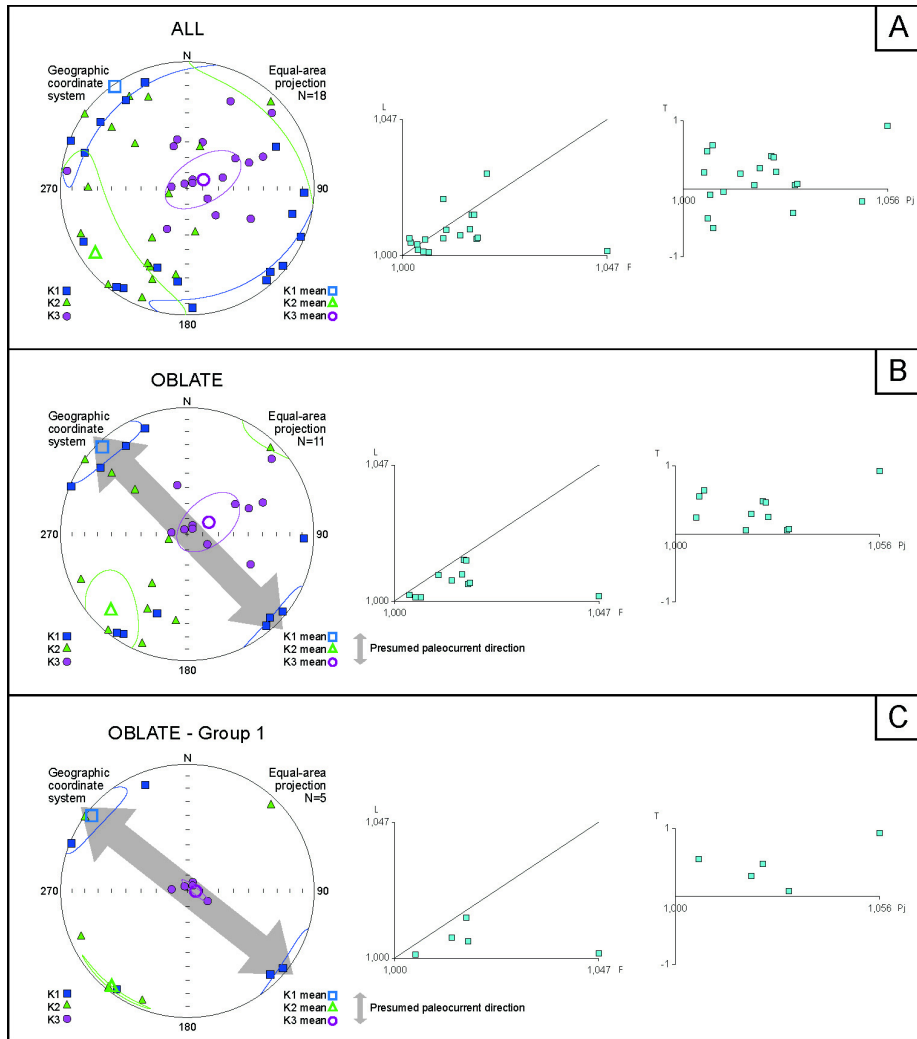


Figure 9: Equal-area projection stereogram (left-hand side) of the anisotropy axes K1, K2 and K3 (with $K_1 > K_2 > K_3$) and Flinn and Jelinek plots (right-hand side) for a) all the samples; b) samples with oblate-shaped anisotropy ellipsoid; c) samples with K_3 imbrication angle less than $20-25^\circ$.

the *C. etruscus*, BM3 includes the medium-sized Cervidae and *Ursus etruscus*, BM4 the medium- and large-sized *Equus* sp., *Bison* sp. and the large-sized cervid *Praemegaceros* sp. Notably, the Voorhies Group III is represented in Fig. 10b only by the crania of the carnivores *Canis* and *Ursus*. Moreover, the fossil record of *U. etruscus* included maxilla fragments (Voorhies Group II/III), isolated teeth, 2 articulated vertebrae and an ulna fragment. Specimens from the BM4 grouped mostly in II/III, II, I/II and showed lack of Voorhies Group I and III. On the other hand, the bulk of undetermined BM specimens plotted in Voorhies Group I/II, with some occurrence in Group I, II, and to a less extent in Group II/III.

Fig. 10c shows the side-by-side distribution of complete and fragmented isolated macromammal skeletal elements. Firstly, the skeletal element distribution of complete specimens suggests a very high teeth/vertebra ratio (7.8). The ratio (3) is lower, but still relatively high when considering isolated, fragmented specimens. Limb bone and undetermined fragments represent the majority of the fragmented, isolated specimens, as compared to axial skeletal parts.

Accordingly, the prominent presence of appendicular skeletal elements over axial is also showed in the distribution of articulated specimens (Fig. 10d), which account for 22% of the sampled assemblage. Articulated lower limb elements (metapodes, carpals/tarsals, phalanges) represent the majority of bones, often articulated to fragmented upper elements (radii, tibiae, humeri, femora). Interestingly, some of the latter elements bear carnivore gnawing marks (Fig. 2e).

4.5. Micromorphology

The TVB-Z 1 block (Fig. 3) consists mostly of poorly sorted sandy silts, compositionally dominated by metamorphic quartz and accessory metamorphic minerals. From base to top, several sharp grain size breaks occur, which partition the sampled interval into mm-thick normally graded laminae, displaying an upward increase of matrix content (Fig. 11a). This includes clay infilling pore spaces (Fig. 11a) and suggests either flow velocity fluctuations or multiple waning depositional events. Birefringent illuvial clay coatings are also present along some voids (Fig. 11b), thus indicating incipient pedogenesis, likely due to temporary subaerial exposure (Kühn et al., 2010).

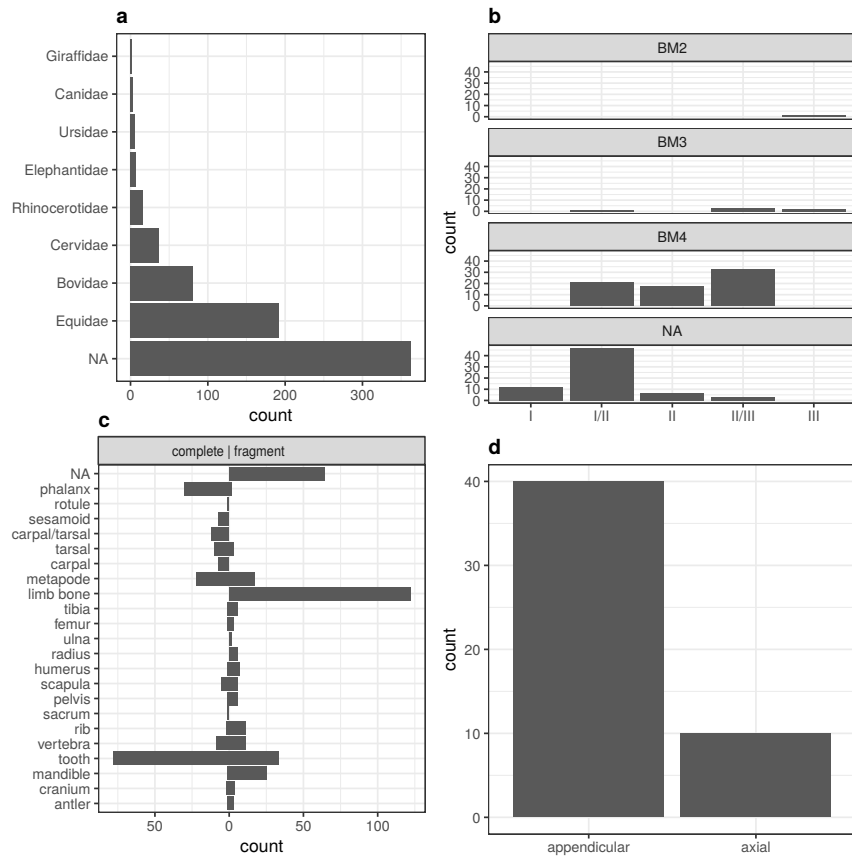


Figure 10: Distribution at the family level of the whole sampled material (a). Voorhies Groups distribution of the complete, isolated macromammal bones (plus rami of mandibles and maxillae) by body mass (BM) (b). Side-by-side distribution of complete/fragmented isolated macromammal skeletal elements (c). Skeletal region distribution of articulated macromammal specimens (d).

543 Most of the thickness of the TVB-Z 2 block (Fig. 3) displays similar characteristics
544 to the TVB-Z 1 block, except for the presence of rolled soil clasts (pedorelicts;
545 Fig. 11c), likely eroded from nearby locations (Cremaschi et al., In press). Conversely,
546 the topmost part of the sample (Fig. 11d) displays moderate clay illuviation along
547 voids, sparse voids most likely related to bioturbation and impregnating redoximor-
548 phic features (Lindbo et al., 2010). The latter include Fe oxide hypocoatings on the
549 groundmass, Fe/Mn oxide nodules with regular outline developed on quartz grains,
550 and fragmented clay coatings. Altogether, these features suggest that, after deposition,
551 Geo 2a has undergone moderate pedogenesis due to a relatively prolonged phase of
552 subaereal exposure in a warm and possibly humid climate or while still saturated with
553 water.

554 5. Discussion

555 Spatial taphonomy has recently emerged as a new methodological framework com-
556 plement to the traditional taphonomic approach (Domínguez-Rodrigo et al., 2017). By
557 using spatial statistical methods, spatial taphonomy aims to investigate the multiscale
558 and multilevel spatial properties of different taphonomic entities (*sensu* Fernández-
559 López, 2006). Indeed, taphonomic alteration processes work simultaneously, at dif-
560 ferent scales, on entities of different level of organisation, from the basic taphonomic
561 elements (bone specimens), to higher level taphonomic groups (taphons) or popula-
562 tions (assemblages). For example, dispersion processes of taphonomic elements may
563 modify their spatial location, orientation and removal degree. At the same time, disper-
564 sion of taphonomic elements may also cause changes in the density, spatial distribution
565 and representatives of elements of each taphon or taphonic population (Fernández-
566 López, 2006). Thus, beside the traditional taphonomic approach, the results of spatial
567 taphonomy are of great importance for investigating the natural or cultural processes
568 of dispersal and accumulation of faunal or cultural remains, in turn with consequences
569 for palaeoecological reconstructions, biochronological estimates and past human be-
570 havioural inferences.

571 In this regard, this study offers an initial contribution to the development of a so far

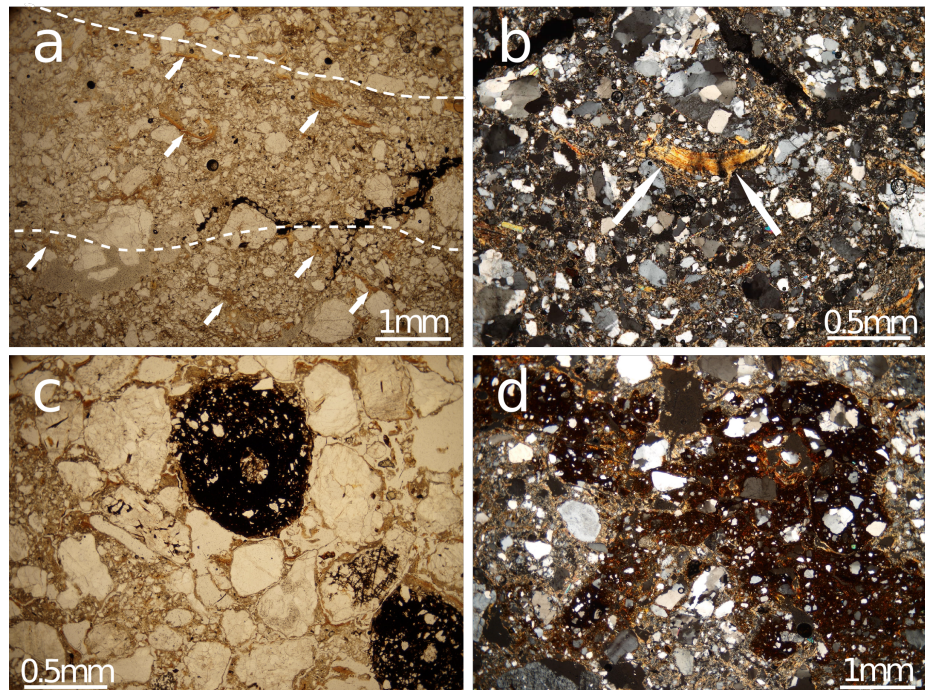


Figure 11: Microphotographs showing a) clast alignments (dashed white lines), crude normal grading and clays infilling pore spaces (arrows) from block TVB-Z 1 in parallel polarized light (PPL); b) illuvial clay coating a planar void from sample TVB-Z 1 in cross polarized light (XPL); c) rolled pedorelict (a Fe/Mn nodule developed on quartz grain) from topmost part of block TVB-Z 2 (PPL); d) Fe oxide hypocoatings on the groundmass and illuvial clay coating of voids from topmost part of block TVB-Z 2 (XPL).

572 non-existent referential framework for the spatial taphonomic interpretation of palaeontological
573 or archaeological assemblages (Domínguez-Rodrigo et al., 2017). Indeed,
574 the taphonomic study of non-human related bone assemblages has great importance
575 for archaeological research as well. As an example, water-flow processes are recog-
576 nised to be among the most important natural processes in the formation and modifi-
577 cation of a significant percentage of the vertebrate fossil and archaeological sites alike
578 (Behrensmeyer, 1975a, 1982, 1988; Coard, 1999; Coard and Dennell, 1995; Petraglia
579 and Nash, 1987; Petraglia and Potts, 1994; Schiffer, 1987; Voorhies, 1969, among
580 others). Under the effect of water-flows, assemblages may adopt a variety of forms,
581 ranging from (peri)autochthonous rearranged assemblages and biased lag assemblages
582 to transported, allochthonous assemblages (Behrensmeyer, 1988; Domínguez-Rodrigo
583 and García-Pérez, 2013). One fundamental assumption behind reliable inferences on
584 past human behaviour is the pristine preservation of the depositional context. There-
585 fore, it is essential, in order to fully comprehend the archaeological record, to test
586 within a referential framework alternative taphonomic hypotheses.

587 In this study, taphonomic dispersion and accumulation processes were analysed
588 focusing on a specific aspect - anisotropy - of the spatial properties of taphonomic enti-
589 ties. A multilevel analysis of anisotropy was conducted at the level of basic taphonomic
590 elements and at the assemblage level. Anisotropy, defined as the preferential orienta-
591 tion of skeletal elements, constitutes a fundamental part of any taphonomic study (Ara-
592 mendi et al., 2017; Benito-Calvo and de la Torre, 2011; Cobo-Sánchez et al., 2014;
593 de la Torre and Benito-Calvo, 2013; Domínguez-Rodrigo et al., 2014a, 2012, 2014d;
594 Fiorillo, 1991; Nash and Petraglia, 1987; Organista et al., 2017; Petraglia and Nash,
595 1987; Petraglia and Potts, 1994; Schick, 1987; Toots, 1965; Voorhies, 1969, among
596 others). However, spatial anisotropy at supra-element level of taphons or assemblages
597 is an often neglected taphonomic criterion that should be reconsidered, especially in
598 spatial taphonomic analyses of fluvial dispersion and accumulation processes. Never-
599 theless, standard spatial statistics rely on crucial assumptions about the isotropy of the
600 spatial processes responsible for the observed spatial pattern (Baddeley et al., 2015).

601 We investigated the multilevel spatial anisotropy and selective composition of the
602 fossiliferous deposit of Tsiotra Vryssi, from the fluvial Gerakarou Formation of the

603 Mygdonia Basin, Greece. Specific research questions regarded the character and num-
604 ber of depositional processes and the degree of re-elaboration of the fossil record. Spe-
605 cific aspects of our results are discussed below.

606 *5.1. Recursive anisotropy*

607 Recursive anisotropy emerged at the level of basic taphonomic elements and at the
608 assemblage level. Fabric analysis, geostatistics, wavelet and point pattern analyses all
609 pointed to a preferential NW-SE orientation of the assemblage and the sub-sample of
610 elongated bone specimens.

611 Fabric analysis, or the analysis of the orientation (plunge and bearing) of elongated
612 elements, can provide valuable insight into taphonomic processes, allowing discrimi-
613 nation between different orientation patterns (isotropic, linear or planar). We analysed
614 a sub-sample of not articulated, clearly elongated bone specimens, mostly limb bone
615 fragments. Articulated units were excluded from the fabric analysis since experimental
616 studies by [Coard and Dennell \(1995\)](#) and [Coard \(1999\)](#) reported that articulated units
617 with a higher number of elements, such as complete limbs, may show weak preferen-
618 tial orientation when not aligned, as they often occur at TSR (Fig. 2c,d,e). Otherwise,
619 the authors concluded that articulated bones showed a greater than expected hydraulic
620 transport potential. Thus, their conspicuous presence in the TSR fossil record (about
621 22%) would not necessarily suggest an autochthonous deposit.

622 The results of the circular uniformity test statistics (Tab. 1) agreed upon rejecting
623 the null hypothesis of uniformity, suggesting a significant anisotropic distribution of the
624 fossil sample. The Schimdt and Woodcock diagrams in Fig. 5 indicated planar fabric
625 (0-to-low degree of dip) and a girdle pattern, with preferential orientation towards the
626 SE. In girdle distribution elements orient over a wider sector of angles than cluster dis-
627 tributions, yet showing higher anisotropy than random distributions. Whereas cluster,
628 linear patterns are associated with channelised water-flows ([Petraglia and Potts, 1994](#)),
629 girdle, planar patterns have been interpreted as products of overland flows (runoff;
630 [Organista et al., 2017](#)). The preferential orientation of the sampled elongated bones
631 suggests that the TSR fossil deposit most likely underwent relatively high-energy, but
632 non-channelised NW-SE water-flows. However, anisotropy does not itself discriminate

633 between allochthonous and autochthonous deposits. Autochthonous lag assemblages
634 undergoing minimal re-sedimentation could also exhibit significant anisotropic spatial
635 patterns (Domínguez-Rodrigo et al., 2012, 2014b, 2017, 2014c). Since a wide range of
636 different taphonomic processes can produce similar patterns, an unequivocal discrim-
637 ination based only on fabric observations is seldom possible, and other taphonomic
638 criteria should be considered (Lenoble and Bertran, 2004).

639 Geostatistics, wavelet and point pattern analyses were applied in order to detect
640 anisotropy of the TSR fossil assemblage. All these different methods agreed on iden-
641 tifying a preferentially NW-SE oriented distribution. Four directional variograms and
642 a variogram map (Fig. 6b,c) were calculated from a kernel density estimation of the
643 assemblage spatial distribution (Fig. 6a). Small, dense clusters of fossils, although
644 occurring at different elevations in the 1m-thick vertical distribution (Fig. 4a), con-
645 catenate along a prevailing NW-SE direction. Secondary minor directions (N-S and
646 NE-SW) were identified in the directional variograms (Fig. 6b). In the same manner,
647 the wavelet graph (Fig. 7) and the rose diagrams (Fig. 8) also detected a strong pref-
648 erential NW-SE directional distribution. Similar elongated lag deposits are typically
649 associated with water-flows dragging material in one direction (Domínguez-Rodrigo
650 et al., 2012).

651 These observations are in agreement with the AMS results. Despite the small sam-
652 ple size, the AMS results suggest relatively strong anisotropy, with a mean K1 axis
653 oriented NW-SE and a mean K2 axis oriented NE-SW, although with much smaller
654 confidence angles (Fig. 9). Since K1 (i.e., the axis of maximum anisotropy) should
655 reflect the bulk orientation of the elongated axis of the ferro/paramagnetic sedimentary
656 particles, it might be concluded that AMS hints at a NW-SE oriented anisotropy.

657 Thus, the observed recursive multilevel anisotropy patterns most probably points
658 to the action of NW-SE oriented water-flows, at the specific location of the TSR site.
659 However, both analyses of isotropy at element level (fabric analysis) and assemblage
660 level (geostatistics, wavelet and point pattern analyses) suggested some degree of noise
661 in the prevalent NW-SE distributions toward other directions, especially to the or-
662 thogonal NE-SW direction. Whereas long bones can roll orthogonally to the main
663 direction of the flow (Voorhies, 1969), noise in the main directional trend at assem-

blage level may indicate multiple depositional processes, or secondary reworking post-depositional processes. Moreover, the relatively high average density of preserved elements ($24/m^2$) occur in small, well defined clusters (Figs. 2f,e, 4 and 6a). Such spatial aggregation of taphonomic elements may be the result of a combination or the sum of different taphonomic processes (Fernández-López et al., 2002). On the other hand, the formation of gaps in the spatial distribution and clusters of elements in correspondence with topographic depression may as well be associated with lag deposits (Petraglia and Potts, 1994). This is likely to happen on top of rippled surfaces or small dunes in the channel-belt. However, there is no evidence of such structure in TSR.

5.2. Differential preservation

According to the evolutionary and systemic theory of taphonomy, taphonomic alteration is not only conceived as a destructive process, but it also has positive effects with the preservation and creation of new taphonomic groups. In this sense, the differential destruction (or taphonomic sieve) of taphonomic entities is just a particular case of taphonomic alteration, as it is the differential modification that gives rise to selective preservation (Fernández-López, 2006). Intrinsic and extrinsic taphonomic factors determine the differential preservation of taphonomic entities. In this study we integrated our spatial taphonomic approach with a preliminary study of the differential preservation of fossil elements.

In the BM4 class of mammals, the relatively high abundance of skeletal elements belonging to the Voorhies Groups I/II, II and II/III (Fig. 10b) suggests minor winnowing of the assemblage, with preservation of the densest elements that are above the threshold of transportability (Behrensmeyer, 1988). Indeed, skeletal elements in the Voorhies Group I (ribs, vertebrae, sacrum, sternum) tend to be transported more easily by saltation or flotation in relatively low-energy currents (Voorhies, 1969). The under-representation of the Voorhies Group III (crania and complete mandibles) in the BM4 class is balanced by the high occurrence of cranial elements in the Group II/III (rami of mandibles and maxilla fragments). Thus, the distribution in Fig. 10b suggests, more than the taphonomic sieve of the Voorhies Group III, a higher fragmentation rate of cranial elements in the BM4 class of mammals (*Equus*, *Bison*, *Praemegaceros*). On

694 the other hand, the Voorhies Group III is better represented in the BM classes 2 and
695 3, which include smaller mammals, i.e., *C. etruscus*, *U. etruscus* and medium-sized
696 cervids. The presence of better preserved carnivore cranial elements, as well as the
697 presence of a partial articulated skeleton of a wolf-sized carnivore, would suggest an
698 autochthonous or para-autochthonous assemblage ([Behrensmeyer, 1988](#)).

699 Although excluded from the Voorhies Group analysis, it is worth noting the pres-
700 ence of several mostly complete skeletal elements of Elephantidae (e.g., ribs, scapula,
701 humerus and several articulated carpals, metacarpals and phalanges) with different FTI
702 values, comparable to elements of the Voorhies Group II and III ([Frison and Todd,](#)
703 [1986](#)). Their distribution suggests that the assemblage was winnowed of the elements
704 with highest FTI, which are comparable to elements of the Voorhies Group I. This is
705 also the case for the other excluded megaherbivore, the rhinocerotid *Stephanorhinus*,
706 which is represented by several teeth and limb bones.

707 Overall, the very high teeth/vertebra ratio (7.8) also supports the hypothesis of a lag,
708 winnowed assemblage. Moreover, the actual presence of a high number of limb and
709 undetermined bone fragments, together with complete appendicular and axial elements
710 (Fig. 10c) supports also some degree of sorting (taphonomic sieve) of the smallest,
711 cancellous fragments. Segregation of axial elements from epiphyses and shafts has
712 been observed even in low-energy fluvial environments ([Domínguez-Rodrigo et al.,](#)
713 [2017](#)).

714 On the other hand, as noted earlier, the conspicuous presence of articulated spec-
715 imens in the TSR fossil assemblage does not necessarily suggest an autochthonous
716 deposition, since articulated bones may as well show a great hydraulic transport po-
717 tential ([Coard, 1999](#); [Coard and Dennell, 1995](#)). Nevertheless, it is worth noting that
718 the distribution of articulated units in TSR shows a significant presence of appendicu-
719 lar elements over axial ones (Fig. 10d). Thus, the under-representation of articulated
720 axial elements also indicates a winnowed, lag assemblage formed by the densest and
721 most resilient elements, with sieve and transport of part of the lighter and more can-
722 cellous elements. However, carnivore ravaging alike tends to eliminate or at least lead
723 to under-representation of those skeletal elements (the less dense, axial elements) in
724 the transport group most prone to be transported by water ([Domínguez-Rodrigo et al.,](#)

725 2012; Voorhies, 1969). Interestingly, a preliminary analysis of the bone breakage pat-
726 terns suggests that carnivores had some active role in the modification and possibly in
727 the accumulation of bones at TSR (Fig. 2e; Konidaris et al., 2015).

728 In conclusion, considering the results of our spatial taphonomic analysis, pro-
729 cesses of taphonomic dispersion, such as fluvial accumulation processes, would have
730 likely separated and disseminated the most cancellous taphonomic elements, favouring
731 the persistence of taphons constituted by allochthonous elements (Fernández-López,
732 2006). Carnivores could have likely been primary accumulation agents. However, the
733 recursive anisotropic spatial patterns, at the level of taphonomic elements and at the
734 assemblage level, as well as the clustering pattern in relatively small, dense, aggre-
735 gations of elements aligned in parallel NW-SE oriented bands, suggest that the TSR
736 deposit resulted from multiple taphonomic dispersion events, with winnowing of less
737 dense, lighter elements and spatial anisotropic re-arrangement of a lag, autochthonous
738 assemblage accumulated over the migrating banks of a NW-SE oriented fluvial system.
739 As suggested by Organista et al. (2017), it is likely for secondary over-bank flows to
740 aggregate bones dispersed over the bank surface into topographic depressions, where
741 they accumulate and acquire greater stability.

742 Noteworthy, both Geo 1 and Geo 2 show fining upward trends and facies sequences
743 similar to those typical of braided rivers (Miall, 1977). In such a sequence, the lower
744 coarser-grained part would represent one or more sets of sinuous-crested medium-scale
745 bedforms (i.e., small dunes) forming by bedload traction in the deeper reaches of chan-
746 nels, whereas the upper muddy part is dominantly deposited by decantation either on
747 top of in-channel or bank-attached emerging bars or in floodplains, occasionally pro-
748 vided with coarse material at high-water stages (Miall, 1982). Therefore, the excavated
749 section can be viewed as the product of cyclical lateral switching of a braided fluvial
750 system.

751 **6. Conclusions**

752 Spatial taphonomy is the systemic, multiscale and multilevel study of the spatial
753 properties of taphonomic processes. Indeed, taphonomic alteration processes work

754 simultaneously, at different scales, on entities of different levels of organisation, from
755 the basic taphonomic elements (bone specimens), to higher level taphonomic groups
756 (taphons) or populations (assemblages). In this study we elaborated on a specific aspect
757 - anisotropy - of the spatial properties of taphonomic processes, investigating an often
758 neglected aspect of the spatial distribution of taphonomic populations.

759 A multilevel analysis of anisotropy was conducted for the Early Pleistocene fossil-
760 iferous locality Tsiotra Vryssi, from the fluvial Gerakarou Formation of the Mygdonia
761 Basin, Greece. Differential preservation of skeletal elements was also analysed in or-
762 der to unravel the character and number of depositional processes and the degree of
763 re-elaboration of the TSR fossil record. The results of the analyses suggested repeated
764 taphonomic dispersion processes, with winnowing of less dense, lighter elements and
765 spatial anisotropic re-arrangement of a lag, autochthonous assemblage possibly accu-
766 mulated over the migrating banks of a NW-SE oriented fluvial system.

767 We believe that this study contributes towards the development of a referential
768 framework for the spatial taphonomic interpretation of other palaeontological, as well
769 as archaeological, localities.

770 Acknowledgements

771 This research was supported by the European Research Council [ERC StG PaGE
772 'Paleoanthropology at the Gates of Europe: Human evolution in the southern Balkans'
773 283503, 2014] and [ERC CoG CROSSROADS 'Human Evolution at the Crossroads'
774 724703, 2017] awarded to K. Harvati. We are grateful to all the participants in the
775 survey and excavation campaigns that took place in the Mygdonia Basin for their in-
776 dispensable contribution.

777 References

778 Aramendi, J., Uribelarrea, D., Arriaza, M. C., Arráiz, H., Barboni, D., Yravedra, J.,
779 Ortega, M. C., Gidna, A., Mabulla, A., Baquedano, E., Domínguez-Rodrigo, M.,
780 2017. The paleoecology and taphonomy of AMK (Bed I, Olduvai Gorge) and its
781 contributions to the understanding of the "Zinj" paleolandscape. Palaeogeography,

- 782 Palaeoclimatology, Palaeoecology 488, 35–49.
- 783 URL [http://www.sciencedirect.com/science/article/pii/
S0031018216308112](http://www.sciencedirect.com/science/article/pii/S0031018216308112)
- 785 Baddeley, A., Rubak, E., Turner, R., 2015. Spatial Point Patterns: Methodology and
786 Applications with R. Chapman and Hall/CRC, London.
- 787 URL <http://www.crcpress.com/books/details/9781482210200/>
- 788 Balsey, J. R., Buddington, A. F., 1960. Magnetic susceptibility anisotropy and fabric
789 of some adirondack granites and orthogneisses. American Journal of Science 258,
790 6–20.
- 791 Behrensmeyer, A., 1975a. Taphonomy and paleoecology in the hominid fossil record.
792 Yearbook of Physical Anthropology 19, 36–50.
- 793 Behrensmeyer, A. K., 1975b. The taphonomy and paleoecology of Plio-Pleistocene
794 vertebrate assemblages East of Lake Rudolf, Kenya. Bulletin of the Museum of
795 Comparative Zoology 146, 473–578.
- 796 Behrensmeyer, A. K., 1982. Time resolution in fluvial vertebrate assemblages. Paleobi-
797 ology 8 (3), 211–227.
- 798 Behrensmeyer, A. K., 1988. Vertebrate preservation in fluvial channels. Palaeogeogra-
799 phy, Palaeoclimatology, Palaeoecology 63 (1), 183–199.
- 800 URL [http://www.sciencedirect.com/science/article/pii/
003101828890096X](http://www.sciencedirect.com/science/article/pii/003101828890096X)
- 802 Benito-Calvo, A., de la Torre, I., 2011. Analysis of orientation patterns in Olduvai
803 Bed I assemblages using GIS techniques: Implications for site formation processes.
804 Journal of Human Evolution 61 (1), 50–60.
- 805 URL [http://www.sciencedirect.com/science/article/pii/
S0047248411000649](http://www.sciencedirect.com/science/article/pii/S0047248411000649)
- 807 Benito-Calvo, A., Martínez-Moreno, J., Mora, R., Roy, M., Roda, X., 2011. Trampling
808 experiments at Cova Gran de Santa Linya, Pre-Pyrenees, Spain: their relevance for

- 809 archaeological fabrics of the Upper–Middle Paleolithic assemblages . Journal of
810 Archaeological Science 38 (12), 3652–3661.
- 811 URL [http://www.sciencedirect.com/science/article/pii/
812 S0305440311003153](http://www.sciencedirect.com/science/article/pii/S0305440311003153)
- 813 Bertran, P., Texier, J.-P., 1995. Fabric Analysis: Application to Paleolithic Sites.
814 Journal of Archaeological Science 22 (4), 521–535.
- 815 URL [http://www.sciencedirect.com/science/article/pii/
816 S0305440385700507](http://www.sciencedirect.com/science/article/pii/S0305440385700507)
- 817 Bevan, A., Conolly, J., 2009. Modelling spatial heterogeneity and nonstationarity in
818 artifact-rich landscapes. Journal of Archaeological Science 36 (4), 956–964.
- 819 URL [http://www.sciencedirect.com/science/article/pii/
820 S0305440308002653](http://www.sciencedirect.com/science/article/pii/S0305440308002653)
- 821 Boaz, D. D., 1982. Modern riverine taphonomy: its relevance to the interpretation of
822 Plio-Pleistocene hominid paleoecology in the Omo basin, Ethiopia. Ph.D. thesis.
- 823 Boaz, N. T., Behrensmeyer, A. K., 1976. Hominid taphonomy: Transport of human
824 skeletal parts in an artificial fluvial environment. American Journal of Physical
825 Anthropology 45 (1), 53–60.
- 826 URL <http://dx.doi.org/10.1002/ajpa.1330450107>
- 827 Coard, R., 1999. One bone, two bones, wet bones, dry bones: Transport potentials
828 under experimental conditions. Journal of Archaeological Science 26 (11), 1369–
829 1375.
- 830 URL [http://www.sciencedirect.com/science/article/pii/
831 S0305440399904387](http://www.sciencedirect.com/science/article/pii/S0305440399904387)
- 832 Coard, R., Dennell, R., 1995. Taphonomy of some articulated skeletal remains:
833 Transport potential in an artificial environment. Journal of Archaeological Science
834 22 (3), 441–448.
- 835 URL [http://www.sciencedirect.com/science/article/pii/
836 S030544038570043X](http://www.sciencedirect.com/science/article/pii/S030544038570043X)

- 837 Cobo-Sánchez, L., Aramendi, J., Domínguez-Rodrigo, M., 2014. Orientation patterns
838 of wildebeest bones on the lake Masek floodplain (Serengeti, Tanzania) and their
839 relevance to interpret anisotropy in the Olduvai lacustrine floodplain. Quaternary
840 International 322–323 (0), 277–284, the Evolution of Hominin Behavior during the
841 Oldowan-Acheulian Transition: Recent Evidence from Olduvai Gorge and Peninj
842 (Tanzania).
- 843 URL [http://www.sciencedirect.com/science/article/pii/
844 S1040618213005363](http://www.sciencedirect.com/science/article/pii/S1040618213005363)
- 845 Cremaschi, M., Trombino, L., Zerboni, A., In press. Palaeosoils and relict soils, a
846 systematic review. In: Stoops, G., Marcelino, V., Mees, F. (Eds.), Interpretation
847 of micromorphological features of soils and regoliths – Revised Edition. Elsevier,
848 Oxford, pp. 873–904.
- 849 Dale, M., Fortin, M., 2014. Spatial Analysis: A Guide for Ecologists, second edition
850 Edition. Cambridge University Press.
- 851 de la Torre, I., Benito-Calvo, A., 2013. Application of GIS methods to retrieve
852 orientation patterns from imagery; a case study from Beds I and II, Olduvai Gorge
853 (Tanzania). Journal of Archaeological Science 40 (5), 2446–2457.
- 854 URL [http://www.sciencedirect.com/science/article/pii/
855 S0305440313000113](http://www.sciencedirect.com/science/article/pii/S0305440313000113)
- 856 Domínguez-Rodrigo, M., Bunn, H., Mabulla, A., Baquedano, E., Uribelarrea,
857 Pérez-González, A., Gidna, A., Yravedra, J., Diez-Martin, F., Egeland, C.,
858 Barba, R., Arriaza, M., Organista, E., Ansón, M., 2014a. On meat eating and
859 human evolution: A taphonomic analysis of BK4b (Upper Bed II, Olduvai Gorge,
860 Tanzania), and its bearing on hominin megafaunal consumption . Quaternary
861 International 322–323, 129–152, the Evolution of Hominin Behavior during the
862 Oldowan-Acheulian Transition: Recent Evidence from Olduvai Gorge and Peninj
863 (Tanzania).
- 864 URL [http://www.sciencedirect.com/science/article/pii/
865 S1040618213006198](http://www.sciencedirect.com/science/article/pii/S1040618213006198)

- 866 Domínguez-Rodrigo, M., Bunn, H., Pickering, T., Mabulla, A., Musiba, C., Baque-
867 dano, E., Ashley, G., Diez-Martin, F., Santonja, M., Uribelarrea, D., Barba, R.,
868 Yravedra, J., Barboni, D., Arriaza, C., Gidna, A., 2012. Autochthony and orientation
869 patterns in Olduvai Bed I: a re-examination of the status of post-depositional biasing
870 of archaeological assemblages from FLK North (FLKN). Journal of Archaeological
871 Science 39 (7), 2116–2127.
- 872 URL [http://www.sciencedirect.com/science/article/pii/
873 S030544031200091X](http://www.sciencedirect.com/science/article/pii/S030544031200091X)
- 874 Domínguez-Rodrigo, M., Bunn, H. T., Yravedra, J., 2014b. A critical re-evaluation of
875 bone surface modification models for inferring fossil hominin and carnivore inter-
876 actions through a multivariate approach: Application to the FLK Zinj archaeofaunal
877 assemblage (Olduvai Gorge, Tanzania). Quaternary International 322–323 (0), 32–
878 43, the Evolution of Hominin Behavior during the Oldowan-Acheulian Transition:
879 Recent Evidence from Olduvai Gorge and Peninj (Tanzania).
- 880 URL [http://www.sciencedirect.com/science/article/pii/
881 S104061821300760X](http://www.sciencedirect.com/science/article/pii/S104061821300760X)
- 882 Domínguez-Rodrigo, M., Cobo-Sánchez, L., Yravedra, J., Uribelarrea, D., Arriaza, C.,
883 Organista, E., Baquedano, E., 2017. Fluvial spatial taphonomy: a new method for the
884 study of post-depositional processes. Archaeological and Anthropological Sciences,
885 1–21.
- 886 URL <http://dx.doi.org/10.1007/s12520-017-0497-2>
- 887 Domínguez-Rodrigo, M., Diez-Martín, F., Yravedra, J., Barba, R., Mabulla, A.,
888 Baquedano, E., Uribelarrea, D., Sánchez, P., Eren, M. I., 2014c. Study of the
889 SHK Main Site faunal assemblage, Olduvai Gorge, Tanzania: Implications for Bed
890 II taphonomy, paleoecology, and hominin utilization of megafauna. Quaternary
891 International 322–323, 153–166.
- 892 URL [http://www.sciencedirect.com/science/article/pii/
893 S104061821300743X](http://www.sciencedirect.com/science/article/pii/S104061821300743X)

- 894 Domínguez-Rodrigo, M., Fernández-López, S., Alcalá, L., 2011. How Can Taphonomy Be Defined in the XXI Century? *Journal of Taphonomy* 9 (1), 1–13.
- 895
- 896 Domínguez-Rodrigo, M., García-Pérez, A., 07 2013. Testing the Accuracy of Different
897 A-Axis Types for Measuring the Orientation of Bones in the Archaeological and
898 Paleontological Record. *PLoS ONE* 8 (7), e68955.
899 URL <http://dx.doi.org/10.1371%2Fjournal.pone.0068955>
- 900 Domínguez-Rodrigo, M., Uribelarrea, D., Santonja, M., Bunn, H., García-Pérez,
901 A., Pérez-González, A., Panera, J., Rubio-Jara, S., Mabulla, A., Baquedano, E.,
902 Yravedra, J., Diez-Martín, F., 2014d. Autochthonous anisotropy of archaeological
903 materials by the action of water: experimental and archaeological reassessment
904 of the orientation patterns at the Olduvai sites. *Journal of Archaeological Science*
905 41 (0), 44–68.
906 URL <http://www.sciencedirect.com/science/article/pii/S0305440313002756>
- 907
- 908 Eberth, D. A., Rogers, R. R., Fiorillo, A. R., 2007. A practical approach to the study of
909 bonebeds. In: Rogers, R. R., Eberth, D. A., Fiorillo, A. R. (Eds.), *Bonebeds. Genesis,*
910 *Analysis, and Paleobiological Significance*. The University of Chicago Press, pp.
911 265–332.
- 912 Efremov, I. A., 1940. Taphonomy: a new branch of paleontology. *Pan American
913 Geologist* 74, 81–93.
914 URL http://www.academia.dk/BiologiskAntropologi/Tafonomi/Efremov_1940.php
915
- 916 Felletti, F., Dall’Olio, E., Muttoni, G., 2016. Determining flow directions in turbidites:
917 An integrates sedimentological and magnetic fabric study of the Miocene Marnoso
918 Arenacea Formation (northern Apennines, Italy). *Sedimentary Geology* 335, 197–
919 215.
- 920 Fernández-Jalvo, Y., Scott, L., Andrews, P., 2011. Taphonomy in palaeoecological
921 interpretations. *Quaternary Science Reviews* 30 (11), 1296–1302.

- 922 URL [http://www.sciencedirect.com/science/article/pii/
S0277379110002842](http://www.sciencedirect.com/science/article/pii/S0277379110002842)
- 924 Fernández-López, R. S., Fernández-Jalvo, Y., Alcalá, L., 2002. Accumulation: taphonomic concept and other palaeontological uses. In: Renzi, M. D., Alonso, M. P., Belinchón, M., Peñalver, E., Montoya, P., Márquez-Aliaga, A. (Eds.), Current Topics on Taphonomy and Fossilization. pp. 37–47.
- 928 Fernández-López, S., 2006. Taphonomic alteration and evolutionary taphonomy. Journal of Taphonomy 4 (3), 111–142.
- 930 Fiorillo, A. R., 1988. A proposal for graphic presentation of orientation data from
931 fossils. Contributions to Geology 26 (1), 1–4.
- 932 Fiorillo, A. R., 1991. Taphonomy and depositional setting of Careless Creek Quarry
933 (Judith River Formation), Wheatland County, Montana, U.S.A. Palaeogeography,
934 Palaeoclimatology, Palaeoecology 81 (3), 281–311.
- 935 URL [http://www.sciencedirect.com/science/article/pii/
003101829190151G](http://www.sciencedirect.com/science/article/pii/003101829190151G)
- 937 Frison, G. C., Todd, L. C., 1986. The Colby Mammoth Site: Taphonomy and Archaeology of a Clovis Kill in Northern Wyoming. University of New Mexico Press.
- 939 Giusti, D., Arzarello, M., 2016. The need for a taphonomic perspective in spatial
940 analysis: Formation processes at the Early Pleistocene site of Pirro Nord (P13),
941 Apricena, Italy. Journal of Archaeological Science: Reports 8, 235–249.
- 942 URL [http://www.sciencedirect.com/science/article/pii/
S2352409X16302656](http://www.sciencedirect.com/science/article/pii/S2352409X16302656)
- 944 Giusti, D., Tourloukis, V., Konidaris, G., Thompson, N., Karkanas, P., Panagopoulou,
945 E., Harvati, K., in press. Beyond maps: Patterns of formation processes at the
946 Middle Pleistocene open-air site of Marathousa 1, Megalopolis basin, Greece.
947 Quaternary International.
- 948 URL [https://www.sciencedirect.com/science/article/pii/
S1040618217309795](https://www.sciencedirect.com/science/article/pii/S1040618217309795)

- 950 Hamilton, N., Rees, A. J., 1970. The use of magnetic fabric in palaeocurrent estimation.
951 In: Runcorn, S. K. (Ed.), Palaeogeophysics. Academic, London, pp. 445–464.
- 952 Hill, A., 1976. On carnivore and weathering damage to bone. Current Anthropology
953 17, 335–336.
- 954 Hrouda, F., 1982. Magnetic anisotropy of rocks and its application in geology and
955 geophysics. Geophysical Surveys 5 (1), 37–82.
- 956 Hrouda, F., Janák, F., 1976. The changes in shape of the magnetic susceptibility ellip-
957 soid during progressive metamorphism and deformation. Tectonophysics 34, 135–
958 148.
- 959 Jammalamadaka, S., Sengupta, A., Sengupta, A., 2001. Topics in Circular Statistics.
960 Series on multivariate analysis. World Scientific.
961 URL <https://books.google.de/books?id=sKqWMGqQXQkC>
- 962 Jelinek, V., 1981. Characterization of the magnetic fabrics of rocks. Tectonophysics 79,
963 63–67.
- 964 Kaufmann, C., Gutiérrez, M. A., Álvarez, M. C., González, M. E., Massigoge, A.,
965 2011. Fluvial dispersal potential of guanaco bones (*Lama guanicoe*) under con-
966 trolled experimental conditions: the influence of age classes to the hydrodynamic
967 behavior. Journal of Archaeological Science 38 (2), 334–344.
968 URL [http://www.sciencedirect.com/science/article/pii/
969 S0305440310003201](http://www.sciencedirect.com/science/article/pii/S0305440310003201)
- 970 Konidaris, G. E., Kostopoulos, D. S., Koufos, G. D., V., T., Harvati, K., 2016. Tsio-
971 tra Vryssi: a new vertebrate locality from the Early Pleistocene of Mygdonia Basin
972 (Macedonia, Greece). In: XIV Annual Meeting of the European Association of Ver-
973 tebrate Palaeontologists. Koninklijke Nederlandse Akademie Van Wetenschappen,
974 p. 37.
- 975 Konidaris, G. E., Tourloukis, V., Kostopoulos, D. S., Thompson, N., Giusti, D.,
976 Michailidis, D., Koufos, G. D., Harvati, K., 2015. Two new vertebrate localities

- 977 from the Early Pleistocene of Mygdonia Basin (Macedonia, Greece): Preliminary
978 results. Comptes Rendus Palevol 14 (5), 353–362.
- 979 URL [http://www.sciencedirect.com/science/article/pii/
980 S1631068315000706](http://www.sciencedirect.com/science/article/pii/S1631068315000706)
- 981 Koufos, G. D., Konidaris, G. E., Harvati, K., in press. Revisiting *Ursus etruscus*
982 (Carnivora, Mammalia) from the Early Pleistocene of Greece with description of
983 new material. Quaternary International.
- 984 URL [http://www.sciencedirect.com/science/article/pii/
985 S1040618217306985](http://www.sciencedirect.com/science/article/pii/S1040618217306985)
- 986 Koufos, G. D., Syrides, G. E., Kostopoulos, D. S., Koliadimou, K. K., 1995. Pre-
987 liminary results about the stratigraphy and the palaeoenvironment of Mygdonia
988 Basin, Macedonia, Greece. Geobios 28 (Supplement 1), 243–249, first European
989 Palaeontological Congress.
- 990 URL [http://www.sciencedirect.com/science/article/pii/
991 S0016699595801715](http://www.sciencedirect.com/science/article/pii/S0016699595801715)
- 992 Kühn, P., Aguilar, J., Miedema, R., 2010. Textural pedofeatures and related horizons.
993 In: Stoops, G., Marcelino, V., Mees, F. (Eds.), Interpretation of micromorphological
994 features of soils and regoliths. Elsevier, Oxford, pp. 217–250.
- 995 Lanza, R., Meloni, A., 2006. The Earth's Magnetism: An Introduction to Geologists.
996 Springer, Berlin.
- 997 Legendre, P., Legendre, L., 2012. Numerical Ecology. Developments in Environmental
998 Modelling. Elsevier Science.
- 999 Lenoble, A., Bertran, P., 2004. Fabric of Palaeolithic levels: methods and implications
1000 for site formation processes. Journal of Archaeological Science 31 (4), 457 – 469.
- 1001 URL [http://www.sciencedirect.com/science/article/pii/
1002 S0305440303001432](http://www.sciencedirect.com/science/article/pii/S0305440303001432)
- 1003 Lenoble, A., Bertran, P., Lacrampe, F., 2008. Solifluction-induced modifications
1004 of archaeological levels: simulation based on experimental data from a modern

- 1005 periglacial slope and application to French Palaeolithic sites. *Journal of Archaeo-*
1006 *logical Science* 35 (1), 99 – 110.
- 1007 URL [http://www.sciencedirect.com/science/article/pii/
1008 S0305440307000489](http://www.sciencedirect.com/science/article/pii/S0305440307000489)
- 1009 Lindbo, D. L., Stolt, M. H., Vepraskas, M. J., 2010. Redoximorphic features. In:
1010 Stoops, G., Marcelino, V., Mees, F. (Eds.), *Interpretation of micromorphological*
1011 *features of soils and regoliths*. Elsevier, Oxford, pp. 129–147.
- 1012 Liu, B., Saito, Y., Yamazaki, T., Abdelayem, A., Oda, H., Hori, K., Zhao, Q., 2001.
1013 Paleocurrent analysis for the Late Pleistocene-Holocene incised-valley fill of the
1014 Yangtze delta, China by using anisotropy of magnetic susceptibility data. *Marine*
1015 *Geology* 176, 175–189.
- 1016 Lloyd, C., Atkinson, P., 2004. Archaeology and geostatistics. *Journal of Archaeologi-*
1017 *cal Science* 31 (2), 151 – 165.
- 1018 URL [http://www.sciencedirect.com/science/article/pii/
1019 S0305440303001067](http://www.sciencedirect.com/science/article/pii/S0305440303001067)
- 1020 Lowrie, W., Hirt, A. M., 1987. Anisotropy of magnetic susceptibility in the scaglia
1021 rossa pelagic limestone. *Earth and Planetary Science Letters* 82, 349–356.
- 1022 Lyman, R., 1994. *Vertebrate Taphonomy*. Cambridge Manuals in Archaeology. Cam-
1023 bridge University Press.
- 1024 Lyman, R. L., 2010. What taphonomy is, what it isn't, and why taphonomists should
1025 care about the difference. *Journal of Taphonomy* 8 (1), 1–16.
- 1026 Markofsky, S., Bevan, A., 2012. Directional analysis of surface artefact distributions:
1027 a case study from the Murghab Delta, Turkmenistan. *Journal of Archaeological*
1028 *Science* 39 (2), 428 – 439.
- 1029 URL [http://www.sciencedirect.com/science/article/pii/
1030 S030544031100358X](http://www.sciencedirect.com/science/article/pii/S030544031100358X)

- 1031 Miall, A. D., 1977. Lithofacies Types and Vertical Profile Models in Braided River
1032 Deposits: A Summary. In: Miall, A. D. (Ed.), Fluvial Sedimentology. Vol. Memoir
1033 5. Canadian Society of Petroleum Geologists, Calgary, pp. 597–604.
- 1034 Miall, A. D., 1982. Analysis of fluvial depositional systems. AAPG, Tulsa, Okla.
- 1035 Murphy, C. P., 1986. Thin section preparation of soils and sediments. AB Academic
1036 Publishers, Berkhamsted.
- 1037 Nash, D. T., Petraglia, M. D. (Eds.), 1987. Natural formation processes and the archaeo-
1038 logical record. Vol. 352 of International Series. British Archaeological Reports,
1039 Oxford.
- 1040 Novak, B., Housen, B., Kitamura, Y., Kanamatsuc, T., Kawamura, K., 2014. Magnetic
1041 fabric analyses as a method for determining sediment transport and deposition in
1042 deep sea sediments. Marine Geology 356, 19–30.
- 1043 Organista, E., Domínguez-Rodrigo, M., Yravedra, J., Uribelarrea, D., Arriaza, M. C.,
1044 Ortega, M. C., Mabulla, A., Gidna, A., Baquedano, E., 2017. Biotic and abiotic
1045 processes affecting the formation of {BK} Level 4c (Bed II, Olduvai Gorge) and
1046 their bearing on hominin behavior at the site. Palaeogeography, Palaeoclimatology,
1047 Palaeoecology 488, 59–75.
- 1048 URL [http://www.sciencedirect.com/science/article/pii/
1049 S0031018216306800](http://www.sciencedirect.com/science/article/pii/S0031018216306800)
- 1050 Palombo, M. R., 2010. A scenario of human dispersal in the northwestern Mediter-
1051 ranean throughout the Early to Middle Pleistocene. Quaternary International
1052 223–224 (0), 179–194.
- 1053 URL [http://www.sciencedirect.com/science/article/pii/
1054 S1040618209004145](http://www.sciencedirect.com/science/article/pii/S1040618209004145)
- 1055 Palombo, M. R., 2016. To what extent could functional diversity be a useful tool in
1056 inferring ecosystem responses to past climate changes? Quaternary International
1057 413 (Part B), 15–31.

- 1058 URL [http://www.sciencedirect.com/science/article/pii/
S1040618215007806](http://www.sciencedirect.com/science/article/pii/S1040618215007806)
- 1060 Pante, M. C., Blumenschine, R. J., 2010. Fluvial transport of bovid long bones
1061 fragmented by the feeding activities of hominins and carnivores. Journal of Archaeo-
1062 logical Science 37 (4), 846 – 854.
- 1063 URL [http://www.sciencedirect.com/science/article/pii/
S0305440309004324](http://www.sciencedirect.com/science/article/pii/S0305440309004324)
- 1065 Parés, J. M., Hassold, N. J. C., Rea, D. K., van der Pluijm, B. A., 2007. Paleocurrent di-
1066 rections from paleomagnetic reorientation of magnetic fabrics in deep-sea sediments
1067 at the Antarctic Peninsula Pacific margin (ODP sites 1095, 1101). Marine Geology
1068 242, 261–269.
- 1069 Petraglia, M. D., Nash, D. T., 1987. The impact of fluvial processes on experimen-
1070 tal sites. In: Nash, D. T., Petraglia, M. D. (Eds.), Natural formation processes and
1071 the archaeological record. Vol. 352 of International Series. British Archaeological
1072 Reports, Oxford, pp. 108–130.
- 1073 Petraglia, M. D., Potts, R., 1994. Water Flow and the Formation of Early Pleistocene
1074 Artifact Sites in Olduvai Gorge, Tanzania. Journal of Anthropological Archaeology
1075 13 (3), 228–254.
- 1076 URL [http://www.sciencedirect.com/science/article/pii/
S0278416584710142](http://www.sciencedirect.com/science/article/pii/S0278416584710142)
- 1078 R Core Team, 2017. R: A Language and Environment for Statistical Computing. R
1079 Foundation for Statistical Computing, Vienna, Austria.
1080 URL <https://www.R-project.org/>
- 1081 Rosenberg, M., Anderson, C., 2011. Passage: Pattern analysis, spatial statistics and
1082 geographic exegesis. version 2. Methods in Ecology and Evolution 2 (3), 229–232.
- 1083 Rosenberg, M. S., 2004. Wavelet analysis for detecting anisotropy in point patterns.
1084 Journal of Vegetation Science 15 (2), 277–284.
1085 URL <http://dx.doi.org/10.1111/j.1654-1103.2004.tb02262.x>

- 1086 Schick, K. D., 1987. Experimentally-derived criteria for assessing hydrologic distur-
1087 bance of archaeological sites. In: Nash, D. T., Petraglia, M. D. (Eds.), Natural for-
1088 mation processes and the archaeological record. Vol. 352 of International Series.
1089 British Archaeological Reports, Oxford, pp. 86–107.
- 1090 Schiffer, M. B., 1987. Formation processes of the archaeological record. University of
1091 New Mexico Press, Albuquerque.
- 1092 Stacey, F. D., Joplin, G., Lindsay, J., 1960. Magnetic anisotropy and fabric of some
1093 foliated rocks from se australia. Geofisica Pura e Applicata 47, 30–40.
- 1094 Tarling, D. H., Hrouda, F., 1993. The Magnetic Anisotropy of Rocks. Chapman and
1095 Hall, London.
- 1096 Toots, H., 1965. Orientation and distribution of fossils as environmental indicators. In:
1097 Nineteenth Field Conference of the Wyoming Geological Association. pp. 219–292.
- 1098 Voorhies, M., 1969. Taphonomy and population dynamics of an early Pliocene ver-
1099 tebrate fauna, Knox County, Nebraska. Contributions to Geology, University of
1100 Wyoming Special Paper 1, 1–69.
- 1101 Woodcock, N., Naylor, M., 1983. Randomness testing in three-dimensional orientation
1102 data. Journal of Structural Geology 5 (5), 539 – 548.
- 1103 URL [http://www.sciencedirect.com/science/article/pii/
1104 0191814183900585](http://www.sciencedirect.com/science/article/pii/0191814183900585)